

## Results

As shown in Fig. 2, cbOEF image from DARG protocol has similar image contrast against qOEF image, and better image quality (less noisy and no image artifact outside of the brain) than qOEF image. Comparisons between cbOEF-AI and qOEF-AI were carried out (Fig. 3), and correlation coefficient and slope of the regression line were summarized in Table 1. All plots except cbOEF-AI from 0 to 60 s of  $^{15}\text{O}_2$  summed image have significant correlation ( $P < 0.01$ ) against qOEF-AI. The best correlation coefficient was obtained as 0.94 when cbOEF was calculated from 0 to 180 s of  $^{15}\text{O}_2$  summed image and 340–440 s of  $\text{C}^{15}\text{O}_2$  summed image. However, the slope of the regression line in this case was 0.80, and cbOEF underestimated AI compared with qOEF. The slope of the regression almost became unity when cbOEF was calculated from 60 to 180 s of  $^{15}\text{O}_2$  summed image and 340–390 s of  $\text{C}^{15}\text{O}_2$  summed image.

## Discussion

In this study, we investigated the relationship between cbOEF-AI and qOEF-AI obtained from the DARG protocol. The regression analysis was performed in order to optimize the summation time for  $^{15}\text{O}_2$  phase and  $\text{C}^{15}\text{O}_2$  phase in cbOEF calculation. By selecting the proper summation time, the cbOEF-AI could be utilized for diagnosing unilateral misery perfusion without arterial blood sampling.

The cbOEF image has been widely used with  $^{15}\text{O}$  PET studies due to the simple calculation. Owing to this simplicity, the image quality of cbOEF is better than that of qOEF as shown in Fig. 2. However, since the cbOEF is empirical, in order to use the cbOEF as diagnostic tool, one must take into account of several factors such as radioactivity from blood vessel and recirculation water converted from  $^{15}\text{O}_2$ . The DARG protocol has another factor to be considered. Since the  $\text{C}^{15}\text{O}_2$  gas is inhaled shortly after the  $^{15}\text{O}_2$  gas inhalation in the DARG protocol, the residual radioactivity from  $^{15}\text{O}_2$  gas and recirculation water converted from  $^{15}\text{O}_2$  gas contaminates PET counts during  $\text{C}^{15}\text{O}_2$  phase.

In order to interpret the results of Fig. 3 and Table 1, not only considering count statistics, it is important to consider the physiologic model of  $^{15}\text{O}_2$  and water. As Mintun et al. proposed [13] that the total radioactivity in the tissue after the  $^{15}\text{O}_2$  and  $\text{C}^{15}\text{O}_2$  administration can be expressed as,

$$Ci(t) = f \cdot A_{\text{H}_2\text{O}}(t) \otimes \exp^{-\frac{t}{\tau}} + E \cdot f \cdot A_{\text{O}_2}(t) \otimes \exp^{-\frac{t}{\tau}} + V_B \cdot R_{\text{Hct}}(1 - F_v \cdot E)A_{\text{O}_2}(t) \quad (3)$$

The first term of the right-hand side describes the amount of water entering the tissue. The second term

represents the amount of oxygen that enters the tissue and is immediately metabolized to water. The third term is the radioactivity of the  $^{15}\text{O}_2$  in the blood vessels. After the inhalation of  $^{15}\text{O}_2$  gas, the  $^{15}\text{O}_2$  was metabolized in whole body as time advances, and the radioactivity of recirculation water gradually increases as the first term of the right-hand side of the Eq. 3. In general, the more the radioactivity from the recirculation water contains in the  $\text{O}_2$  phase, the worse the cbOEF-AI correlates against qOEF-AI. As shown in Fig. 3 and Table 1,  $^{15}\text{O}_2$  summation time extended to 240 s resulted in worse correlation than summation time to 180 s due to the influence of the recirculation water. If one compares between the results of the  $\text{C}^{15}\text{O}_2$  summation time of 340–390 s (A) and 390–440 s (B), the slopes of (B) were smaller than (A) although the correlation coefficients for (B) were better than (A) in most cases. The count statistics of (B) was better than (A), which lead better correlation between cbOEF-AI and qOEF-AI. On the other hand, the  $\text{C}^{15}\text{O}_2$  image of (B) has less contrast than (C) due to the diffusability of water, which causes the underestimation of cbOEF-AI against qOEF-AI. Because the  $^{15}\text{O}_2$  image with the summation time of 0–60 s has the poorest count statistics, the cbOEF-AI with  $^{15}\text{O}_2$  the summation time of 0–60 s had the worst correlation against qOEF-AI. Note that the blood component (the third term of Eq. 3) has the large influence on the  $^{15}\text{O}_2$  image with summation time of 0–60 s, and the magnitude of this influence depends on the OEF value, which leads the underestimation of cbOEF-AI against qOEF-AI. Meanwhile, as judged by the best correlation coefficient, we recommend to use the following combinations:

- $^{15}\text{O}_2$  summation time of 0–180 s and  $\text{C}^{15}\text{O}_2$  summation time of 340–440 s
- $^{15}\text{O}_2$  summation time of 60–180 s and  $\text{C}^{15}\text{O}_2$  summation time of 340–390 s

In the latter case, the correlation coefficient was lower than one in the former, but this combination makes it possible to shorten the PET acquisition time.

Kobayashi et al. [25] reported the cbOEF-AI can be successfully used to diagnose misery perfusion if one uses 4–7 min of the summation time for continuous inhalation of  $^{15}\text{O}_2$  gas in addition to 3 min of  $\text{H}_2^{15}\text{O}$  PET acquisition. In their study, the waiting time between  $^{15}\text{O}_2$  scan and  $\text{H}_2^{15}\text{O}$  scan is necessary to avoid contamination of  $^{15}\text{O}_2$  radioactivity in  $\text{H}_2^{15}\text{O}$  data. Hence, the total study time for their study should be longer than 10 min. As shown in this paper, the qOEF-AI equivalent cbOEF-AI will be able to be obtained by 7.3 min after the start of  $^{15}\text{O}_2$  inhalation. By using cbOEF-AI with the DARG protocol, total study time can be dramatically shortened, which is beneficial for patients as well as medical staff, and the cbOEF-AI with

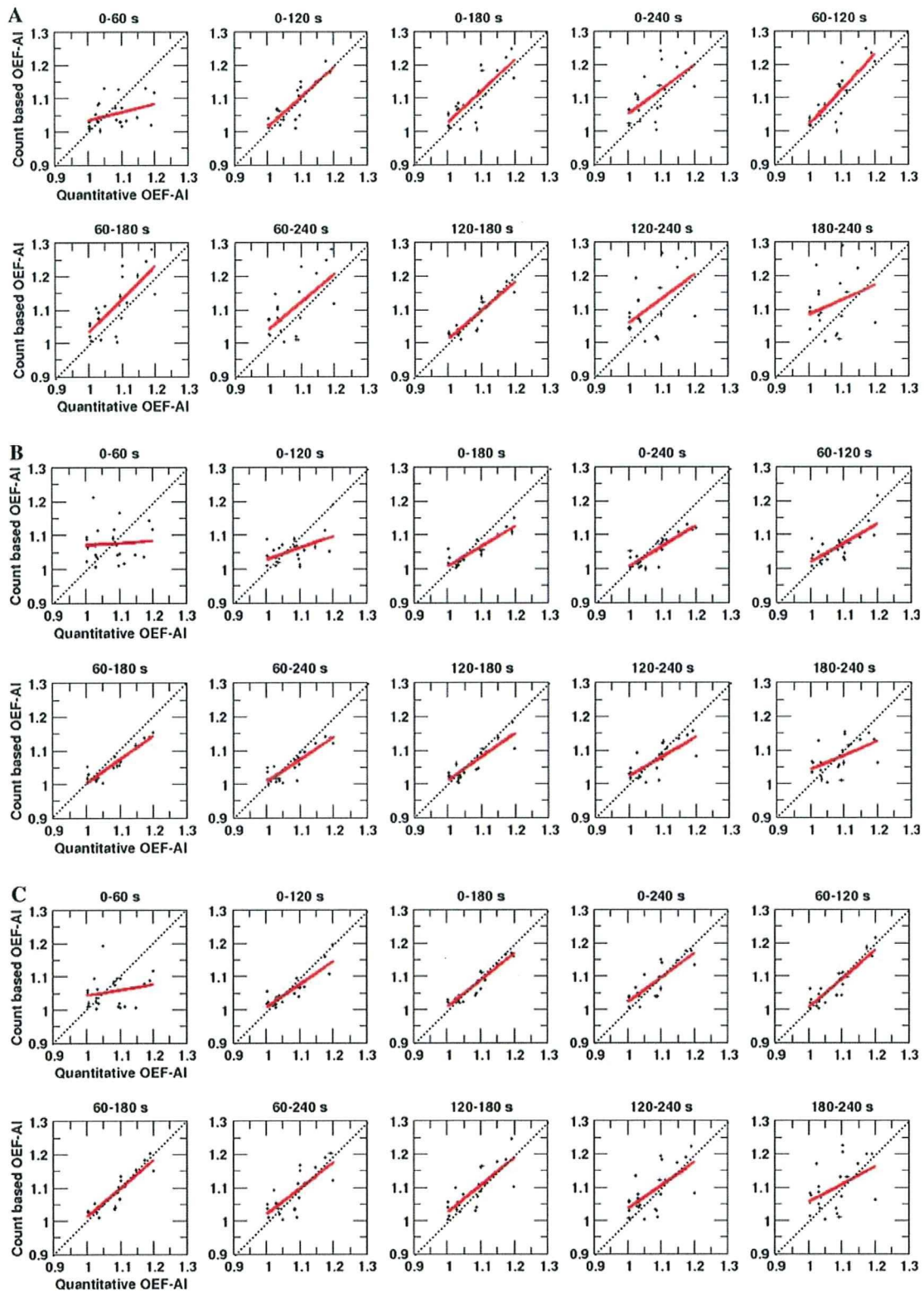


**Fig. 3** These graphs show the correlation between qOEF-AI and cbOEF-AI. Each graph has different summation time for  $^{15}\text{O}_2$  and  $\text{C}^{15}\text{O}_2$  phases in the DARG protocol. The title of each graph represents the summation time for  $^{15}\text{O}_2$  phase. The summation times for  $\text{C}^{15}\text{O}_2$  phase are from 340 to 390 s for (a), 390–440 s for (b), and 340–440 s for (c)

**Table 1** Correlation coefficient, slope and y-intercept between qOEF-AI and cbOEF-AI with different summation periods

O <sub>2</sub> summation time (s)	CO <sub>2</sub> summation time (s)								
	340–390 (A)			390–440 (B)			340–440 (C)		
	Correlation coefficient	Slope	y-Intercept	Correlation coefficient	Slope	y-Intercept	Correlation coefficient	Slope	y-Intercept
0–60	0.35	0.24	0.79	0.06	0.05	1.02	0.21	0.16	0.88
0–120	0.87	0.91	0.10	0.52	0.35	0.68	0.88	0.69	0.31
0–180	0.79	0.94	0.09	0.90	0.59	0.41	0.94	0.80	0.20
0–240	0.59	0.74	0.30	0.86	0.61	0.39	0.83	0.74	0.28
60–120	0.84	1.06	−0.05	0.74	0.57	0.44	0.90	0.87	0.13
60–180	0.75	0.99	0.04	0.93	0.70	0.29	0.91	0.86	0.15
60–240	0.63	0.84	0.19	0.87	0.66	0.34	0.77	0.78	0.24
120–180	0.91	0.86	0.15	0.89	0.70	0.30	0.79	0.82	0.20
120–240	0.51	0.73	0.23	0.75	0.59	0.43	0.64	0.70	0.20
180–240	0.30	0.44	0.64	0.54	0.42	0.61	0.47	0.54	0.51

Time 0 was the <sup>15</sup>O<sub>2</sub> scan start time. The scan for <sup>15</sup>O<sub>2</sub> and C<sup>15</sup>O<sub>2</sub> was the single scan for 480 s

the DARG protocol might be used for acute patients due to its simple and rapid procedure.

As shown in Fig. 1, even though the DARG protocol can be terminated at 7.3 min from <sup>15</sup>O<sub>2</sub> inhalation, our study must have 10 min of transmission scan to correct attenuation of photons. The time duration for the transmission scan is possible to be minimized by segmented attenuation correction techniques [28], or using hybrid PET-CT scanner. Note that for computing cbOEF-AI, no C<sup>15</sup>O scan is required. Kobayashi et al. [24] showed no blood volume correction was required to compute cbOEF-AI, when they used bolus injection of H<sub>2</sub><sup>15</sup>O instead of steady-state protocol.

In this study, we used the DARG protocol with C<sup>15</sup>O<sub>2</sub> inhalation after 6 min from the beginning of <sup>15</sup>O<sub>2</sub> inhalation. The optimal summation time for cbOEF-AI could be different if the time interval between inhalations of <sup>15</sup>O<sub>2</sub> and C<sup>15</sup>O<sub>2</sub> gases is altered. If one is administered C<sup>15</sup>O<sub>2</sub> gas earlier than 6 min, the contamination of <sup>15</sup>O<sub>2</sub> radioactivity on C<sup>15</sup>O<sub>2</sub> phase becomes larger, which will result in changing optimal summation time for cbOEF-AI. Further systematic investigations will be required to obtain more general conclusion, and it might be possible to shorten the total scan duration for proper cbOEF-AI with the DARG protocol. The image quality of PET is also influenced on the results. In our study, all data were obtained in 2D mode. It is not clear that 3D acquisition of PET affects our results. Ibaraki et al showed that qOEF was possible to obtain in 3D acquisition as good as 2D acquisition [29], which suggests the usability of cbOEF in 3D acquisition, although further studies are required to confirm. For computing cbOEF, it is important to assure that a patient does not move during PET acquisition. There are several techniques to compensate the motion of the patient

by means of hardware [30] or software although simplicity of cbOEF-AI is lost by applying these techniques. We blindly selected data from patients, who underwent DARG protocol. Therefore, varieties of patient's history and diagnosis were included, and it is difficult to judge clinical usability of the cbOEF-AI with DARG protocol by our study so far. Clinical impact of cbOEF-AI with DARG protocol is beyond the scope of this paper. We have a plan to evaluate diagnostic accuracy for the present technique in future.

## Conclusion

In this paper, we investigated the feasibility of cbOEF-AI with DARG protocol, and relationship between cbOEF-AI and qOEF-AI by varying the summation time. The cbOEF-AI with the DARG protocol may contribute to diagnose unilateral misery perfusion within 7.3 min.

## References

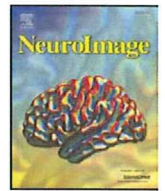
1. Powers WJ. Cerebral hemodynamics in ischemic cerebrovascular disease. *Ann Neurol*. 1991;29:231–40. doi:10.1002/ana.410290302.
2. Baron JC, Boussier MG, Rey A, Guillard A, Comar D, Castaigne P. Reversal of focal "misery-perfusion syndrome" by extracranial arterial bypass in hemodynamic cerebral ischemia: a case study with <sup>15</sup>O positron emission tomography. *Stroke*. 1981;12:454–9.
3. Yamauchi H, Fukuyama H, Nagahama Y, Nabatame H, Nakamura K, Yamamoto Y, et al. Evidence of misery perfusion and risk for recurrent stroke in major cerebral arterial occlusive diseases from PET. *J Neurol Neurosurg Psychiatry*. 1996;61:18–25. doi:10.1136/jnnp.61.1.18.
4. Yamauchi H, Fukuyama H, Nagahama Y, Nabatame H, Ueno M, Nishizawa S, et al. Significance of increased oxygen extraction

- fraction in 5-year prognosis of major cerebral arterial occlusive disease. *J Nucl Med.* 1999;40:1992–8.
5. Grubb RL Jr, Derdeyn CP, Fritsch SM, Carpenter DA, Yundt KD, Videen TO, et al. Importance of hemodynamic factors in the prognosis of symptomatic carotid occlusion. *JAMA.* 1998;280:1055–60. doi:10.1001/jama.280.12.1055.
  6. Derdeyn CP, Grubb RL Jr, Powers WJ. Cerebral hemodynamic impairment: method of measurement and association with stroke risk. *Neurology.* 1999;53:251–9.
  7. Derdeyn CP, Videen TO, Yundt KD, Fritsch SM, Carpenter DA, Grubb RL Jr, et al. Variability of cerebral blood volume and oxygen extraction: stage of cerebral hemodynamic impairment revisited. *Brain.* 2002;125:595–607. doi:10.1093/brain/awf047.
  8. Subramanyam R, Alpert NM, Hoop B Jr, Brownell GL, Yaveras JM. A model for regional cerebral oxygen distribution during continuous inhalation of  $^{15}\text{O}_2$ ,  $\text{C}^{15}\text{O}$ , and  $\text{C}^{15}\text{O}_2$ . *J Nucl Med.* 1978;19:48–53.
  9. Lammertsma AA, Heather JD, Jones T, Frackowiak RS, Lenzi GL. A statistical study of the steady state technique for measuring regional cerebral blood flow and oxygen utilization using  $^{15}\text{O}$ . *J Comput Assist Tomogr.* 1982;6:566–73. doi:10.1097/00004728-198206000-00022.
  10. Correia JA, Alpert NM, Buxton RB, Ackerman RH. Analysis of some errors in the measurement of oxygen extraction and oxygen consumption by the equilibrium inhalation method. *J Cereb Blood Metab.* 1985;5:591–9.
  11. Okazawa H, Yamauchi H, Sugimoto K, Takahashi M, Toyoda H, Kishibe Y, et al. Quantitative comparison of the bolus and steady-state methods for measurement of cerebral perfusion and oxygen metabolism: positron emission tomography study using  $^{15}\text{O}$ -gas and water. *J Cereb Blood Metab.* 2001;21:793–803. doi:10.1097/00004647-200107000-00004.
  12. Okazawa H, Yamauchi H, Sugimoto K, Toyoda H, Kishibe Y, Takahashi M. Effects of acetazolamide on cerebral blood flow, blood volume, and oxygen metabolism: a positron emission tomography study with healthy volunteers. *J Cereb Blood Flow Metab.* 2001;21:1472–9. doi:10.1097/00004647-200112000-00012.
  13. Mintun MA, Raichle ME, Martin WR, Herscovitch P. Brain oxygen utilization measured with O-15 radiotracers and positron emission tomography. *J Nucl Med.* 1984;25(2):177–87.
  14. Iida H, Jones T, Miura S. Modeling approach to eliminate the need to separate arterial plasma in oxygen-15 inhalation positron emission tomography. *J Nucl Med.* 1993;34:1333–40.
  15. Sadato N, Yonekura Y, Senda M, Iwasaki Y, Matoba N, Tamaki N, et al. PET and the autoradiographic method with continuous inhalation of oxygen-15-gas: theoretical analysis and comparison with conventional steady-state methods. *J Nucl Med.* 1993;34:1672–80.
  16. Hatazawa J, Fujita H, Kanno I, Satoh T, Iida H, Miura S, et al. Regional cerebral blood flow, blood volume, oxygen extraction fraction, and oxygen utilization rate in normal volunteers measured by the autoradiographic technique and the single breath inhalation method. *Ann Nucl Med.* 1995;9:15–21.
  17. Shidahara M, Watabe H, Kim KM, Oka H, Sago M, Hayashi T, et al. Evaluation of a commercial PET tomograph-based system for the quantitative assessment of rCBF, rOEF and rCMRO<sub>2</sub> by using sequential administration of  $^{15}\text{O}$ -labeled compounds. *Ann Nucl Med.* 2002;16(5):317–27. doi:10.1007/BF02988616.
  18. Hattori N, Bergsneider M, Wu HM, Glenn TC, Vespa PM, Hovda DA, et al. Accuracy of a method using short inhalation of  $^{15}\text{O}-\text{O}_2$  for measuring cerebral oxygen extraction fraction with PET in healthy humans. *J Nucl Med.* 2004;45:765–70.
  19. Kudomi N, Hayashi T, Teramoto N, Watabe H, Kawachi N, Ohta Y, et al. Rapid quantitative measurement of CMRO<sub>2</sub> and CBF by dual administration  $^{15}\text{O}$ -labeled oxygen and water during a single PET scan—a validation study and error analysis in anesthetized monkeys. *J Cereb Blood Flow Metab.* 2005;25:1209–24. doi:10.1038/sj.jcbfm.9600118.
  20. Jone T, Chesler DA, Ter-Pogossian MM. The continuous inhalation of oxygen-15 for assessing regional oxygen extraction in the brain of man. *Br J Radiol.* 1976;49:339–43.
  21. Derdeyn CP, Videen TO, Simmons NR, Yundt KD, Fritsch SM, Grubb RL Jr, et al. Count-based PET method for predicting ischemic stroke in patients with symptomatic carotid arterial occlusion. *Radiology.* 1999;212:499–506.
  22. Derdeyn CP, Videen TO, Grubb RL Jr, Powers WJ. Comparison of PET oxygen extraction fraction method for the prediction of stroke risk. *J Nucl Med.* 2001;42(8):1195–7.
  23. Ibaraki M, Shimosegawa E, Miura S, Takahashi K, Ito H, Kanno I, et al. PET measurements of CBF, OEF, and CMRO<sub>2</sub> without arterial sampling in hyperacute ischemic stroke: method and error analysis. *Ann Nucl Med.* 2004;18:35–44. doi:10.1007/BF02985612.
  24. Kobayashi M, Okazawa H, Tsuchida T, Kawai K, Fujibayashi Y, Yoneyama Y. Diagnosis of misery perfusion using noninvasive  $^{15}\text{O}$ -gas PET. *J Nucl Med.* 2006;47:1581–6.
  25. Kobayashi M, Kudo T, Tsujikawa T, Isozaki M, Araki Y, Fujibayashi Y, et al. Shorter examination method for the diagnosis of misery perfusion with count-based oxygen extraction fraction elevation in  $^{15}\text{O}$ -gas PET. *J Nucl Med.* 2008;49:242–6. doi:10.2967/jnumed.107.047118.
  26. Kudomi N, Choi E, Yamamoto S, Watabe H, Kim KM, Shidahara M, et al. Development of a GSO detector assembly for a continuous blood sampling system. *IEEE Trans Nucl Sci.* 2003;50(1):70–3. doi:10.1109/TNS.2002.807869.
  27. Kudomi N, Watabe H, Hayashi T, Iida H. Separation of input function for rapid measurement of quantitative CMRO<sub>2</sub> and CBF in a single PET scan with a dual tracer administration method. *Phys Med Biol.* 2007;52(7):1893–908. doi:10.1088/0031-9155/52/7/009.
  28. Xu M, Cutler PD, Luk WK. Adaptive, segmented attenuation correction for whole-body PET imaging. *IEEE Trans Nucl Sci.* 1996;43:331–6. doi:10.1109/23.485974.
  29. Ibaraki M, Miura S, Shimosegawa E, Sugawara S, Mizuta T, Ishikawa A, et al. Quantification of cerebral blood flow and oxygen metabolism with 3-dimensional PET and  $^{15}\text{O}$ : validation by comparison with 2-dimensional PET. *J Nucl Med.* 2007;49:50–9. doi:10.2967/jnumed.107.044008.
  30. Woo SK, Watabe H, Choi Y, Kim KM, Park CC, Bloomfield PM, et al. Sinogram-based motion correction of PET images using optical motion tracking system and list-mode data acquisition. *IEEE Trans Nucl Sci.* 2004;51(3):782–8. doi:10.1109/TNS.2004.829786.



Contents lists available at ScienceDirect

NeuroImage

journal homepage: [www.elsevier.com/locate/ynimg](http://www.elsevier.com/locate/ynimg)

## Quantitative evaluation of changes in binding potential with a simplified reference tissue model and multiple injections of [<sup>11</sup>C]raclopride

Yoko Ikoma<sup>a,b,\*</sup>, Hiroshi Watabe<sup>a</sup>, Takuya Hayashi<sup>a</sup>, Yoshinori Miyake<sup>c</sup>,  
Noboru Teramoto<sup>a</sup>, Kotaro Minato<sup>b</sup>, Hidehiro Iida<sup>a</sup>

<sup>a</sup> Department of Investigative Radiology, National Cardiovascular Center Research Institute, Suita, Osaka, Japan

<sup>b</sup> Graduate School of Information Science, Nara Institute of Science and Technology, Ikoma, Nara, Japan

<sup>c</sup> Department of Radiology and Nuclear Medicine, National Cardiovascular Center Hospital, Suita, Osaka, Japan

### ARTICLE INFO

#### Article history:

Received 20 February 2009

Revised 27 May 2009

Accepted 29 May 2009

Available online xxx

#### Keywords:

Positron emission tomography

[<sup>11</sup>C]raclopride

Dopamine D<sub>2</sub> receptor

Multiple injections

Binding potential

### ABSTRACT

Positron emission tomography (PET) with [<sup>11</sup>C]raclopride is widely used to investigate temporal changes in the dopamine D<sub>2</sub> receptor system attributed to the dopamine release. The simplified reference tissue model (SRTM) can be used to determine the binding potential (BP<sub>ND</sub>) value using the time–activity curve (TAC) of the reference region as input function. However, in assessing temporal changes in BP<sub>ND</sub> using the SRTM, multiple [<sup>11</sup>C]raclopride PET scans are required, and a second scan must be performed after the disappearance of the [<sup>11</sup>C]raclopride administered in the first scan. In this study, we have developed an extended multiple-injection SRTM to estimate the BP<sub>ND</sub> change, from a single PET scan with multiple injections of [<sup>11</sup>C]raclopride, and we have validated this approach by performing numerous simulations and studies on monkeys. In the computer simulations, TACs were generated for dual injections of [<sup>11</sup>C]raclopride, in which binding conditions changed during the scans, and the BP<sub>ND</sub> values before, and after, the second injection were estimated by the proposed method. As a result, the reduction in BP<sub>ND</sub> was correlated, either with the integral of released dopamine, or with the administered mass of raclopride. This method was applied to studies on monkeys, and was capable of determining two identical BP<sub>ND</sub> values when there were no changes in binding conditions. The BP<sub>ND</sub> after the second injection decreased when binding conditions changed due to an increase in administered raclopride. An advantage of the proposed method is the shortened scan period for the quantitative assessment of the BP<sub>ND</sub> change for neurotransmitter competition studies.

© 2009 Elsevier Inc. All rights reserved.

### Introduction

Neuroreceptor imaging using positron emission tomography (PET) and [<sup>11</sup>C]raclopride has made it possible to determine the density of striatal dopamine D<sub>2</sub> receptors *in vivo* (Farde et al., 1985; Köhler et al., 1985; Hall et al., 1988). The binding potential (BP<sub>ND</sub> =  $k_3/k_4$ ) derived from rate constants in a two-tissue compartment model has been used to quantify the receptor binding (Mintun et al., 1984). Endres et al. then developed an extended compartment model, which included the released neurotransmitter concentration, and demonstrated that [<sup>11</sup>C]raclopride binding decreased after the administration of amphetamine, which resulted in the displacement of the raclopride due to competition with increased dopamine (Endres et al., 1997, Carson

et al., 1997). The model showed that the change in BP<sub>ND</sub> between the baseline and the stimulated state was related to the total amount of released dopamine. Applying this theory, it has been shown that amphetamine-related reductions in [<sup>11</sup>C]raclopride-specific binding in patients with schizophrenia was significantly greater than in healthy volunteers (Breier et al., 1997) and that a reduction in [<sup>11</sup>C]raclopride binding was observed while playing a video game which resulted in the release of endogenous dopamine (Koepp et al., 1998). In this competition paradigm, two PET studies are necessary to measure the BP<sub>ND</sub> values of the baseline and competed conditions, and a long study period is required.

On the other hand, single-scan studies with bolus-plus-continuous infusion (B/I) of the tracer, applied for the measurement of reduction in BP<sub>ND</sub> due to an amphetamine challenge, were also performed (Carson et al., 1997, Endres et al., 1997). In these studies, a stimulus was administered during infusion of the tracer, and the change in binding between pre- and post-amphetamine intervention was measured as the tissue-to-plasma concentration ratio at equilibrium. This method enables the direct measurement of receptor-binding

\* Corresponding author. Department of Investigative Radiology, National Cardiovascular Center Research Institute, 5-7-1, Fujishirodai, Suita, Osaka, 565-8565, Japan. Fax: +81 6 6835 5429.

E-mail address: [ikoma@ri.ncvc.go.jp](mailto:ikoma@ri.ncvc.go.jp) (Y. Ikoma).

changes in a single scan. However, the design of the protocol requires that the tracer kinetics attain equilibrium within the measurement period of the pre- and post-amphetamine challenges (Watabe et al., 2000), and dynamic data that does not reach equilibrium may cause systematic errors in the estimates of binding changes (Zhou et al., 2006).

To compute the  $BP_{ND}$  value, the simplified reference tissue model (SRTM) is often used. The SRTM can provide the  $BP_{ND}$  without invasive arterial blood sampling by using a time–activity curve (TAC) of the reference region where specific bindings are negligible (Lammertsma and Hume, 1996). Recently, an extended simplified reference tissue model (ESRTM) was developed in order to quantify the reduction in  $BP_{ND}$  with B/I administration (Zhou et al., 2006). In the ESRTM method, the  $BP_{ND}$  of the SRTM was estimated separately, before and after, the pharmacological challenge during a 90 min scan with B/I administration. The group reported that stimulus-induced  $BP_{ND}$  changes, obtained from equilibrium analysis in the non-equilibrium state, resulted in an underestimation of the reduction in  $BP_{ND}$ , and that this was significantly improved by using the ESRTM. Nonetheless, B/I administration requires the equipment to provide [<sup>11</sup>C]raclopride constantly during the scan, and there are often technical problems.

Kim et al. (2006) developed a method to measure regional cerebral blood flow in pre- and post-pharmacological stress from a single session of single photon emission computed tomography (SPECT) scanning with dual injections of <sup>123</sup>I-iodoamphetamine. In their paper, they showed mathematical derivation for estimating CBF values from two conditions in a single session of SPECT study. By advancing their method, we have developed a method to detect changes in receptor binding using a single session of PET scanning in conjunction with multiple bolus injections of [<sup>11</sup>C]raclopride synthesized once before the scan (Watabe et al., 2006). In our approach, the SRTM was extended to measure the  $BP_{ND}$  of each injection, and we validated this approach by performing numerous simulations and studies on monkeys using PET and [<sup>11</sup>C]raclopride.

**Methods**

*Theory*

The simplified reference tissue model (SRTM) provides  $BP_{ND}$  without arterial blood sampling by eliminating the arterial plasma TAC arithmetically from model equations, by using the TAC of the reference region where specific bindings are negligible. The radioactivity concentration of the target region ( $C_t$ ) is expressed as Eq. (1), using the radioactivity concentration in the reference region ( $C_r$ ), under the assumption that the target and reference regions can be expressed using the one-tissue compartment model and that the ratios of  $K_1$  and  $k_2$  are equal between the target and reference regions (Lammertsma and Hume, 1996).

$$C_t(t) = R_1 C_r(t) + \left( k_2 - \frac{R_1 k_2}{1 + BP_{ND}} \right) e^{-\frac{k_2}{1 + BP_{ND}} t} \otimes C_r(t) \quad R_1 = K_1 / K_1^r \tag{1}$$

where  $K_1$  and  $k_2$  are the rate constants for the transfer from plasma to the displaceable compartment in the target tissue and from the displaceable compartment to plasma, respectively, and  $K_1^r$  is the rate constant for the transfer from plasma to the reference tissue.

We have extended this SRTM to a multiple-injection study. In this approach, the first injection of the radioligand was performed at the time of the scan start, and the  $BP_{ND}$  was measured as a baseline. Next, a second injection was performed simultaneously with a change in binding conditions, and the  $BP_{ND}$  was measured as

a competitive state after the second injection. The  $BP_{ND}$  values before, and after, the second injection, were estimated by the multiple-injection simplified reference tissue model (MI-SRTM) expressed as follows:

$$C_{t1}(t) = R_{11} C_{r1}(t) + \left( k_{21} - \frac{R_{11} k_{21}}{1 + BP_{ND1}} \right) e^{-\frac{k_{21}}{1 + BP_{ND1}} t} \otimes C_{r1}(t)$$

$$C_{t2}(t) = R_{12} C_{r2}(t) + \left( k_{22} - \frac{R_{12} k_{22}}{1 + BP_{ND2}} \right) e^{-\frac{k_{22}}{1 + BP_{ND2}} t} \otimes C_{r2}(t)$$

$$+ (C_{t0} - R_{12} C_{r0}) e^{-\frac{k_{22}}{1 + BP_{ND2}} t} \tag{2}$$

where  $C_{t1}$  and  $C_{t2}$  are the radioactivity concentrations in the target tissue and  $C_{r1}$  and  $C_{r2}$  are the radioactivity concentrations in the reference tissue for the first and second injections, respectively;  $t$  is the time from the first or second injection;  $C_{t0}$  and  $C_{r0}$  are the radioactivity concentrations of the target and reference tissues at the time of the second injection, respectively.

Firstly,  $R_{11}$ ,  $k_{21}$  and  $BP_{ND1}$  were estimated by nonlinear least squares fitting with the iteration of the Gauss–Newton algorithm using data points before the second injection. Next,  $C_{r0}$  was calculated by the interpolation of the measured reference TAC, and  $C_{t0}$  was estimated using Eq. (1) with estimated  $R_{11}$ ,  $k_{21}$  and  $BP_{ND1}$  values. Finally,  $R_{12}$ ,  $k_{22}$ , and  $BP_{ND2}$  were estimated by nonlinear least squares fitting using these  $C_{r0}$  and  $C_{t0}$  values with Eq. (2). In this study using [<sup>11</sup>C]raclopride, the TAC of the cerebellum was used as a reference TAC.

The present method can be used to generate voxel-based parametric maps. In the voxel-based estimation for parametric imaging of ligand–receptor binding,  $R_{11}$ ,  $k_{21}$  and  $BP_{ND1}$  from the first injection and  $R_{12}$ ,  $k_{22}$ , and  $BP_{ND2}$  from the second injection in Eq. (2), were estimated by a basis function method in which the model Eq. (2) is solved using linear least squares for a set of basis functions, which enables the incorporation of parameter bounds (Gunn et al., 1997).

*Simulation analysis*

Three simulation studies were carried out to validate the present approach and to determine: 1) whether the change in  $BP_{ND}$  caused by competition to receptor binding could be detected by the MI-SRTM; 2) how would the time delay between the endogenous dopamine release and [<sup>11</sup>C]raclopride injection affect  $BP_{ND}$  estimates, and 3) what was an optimal scan duration for a reliable  $BP_{ND}$  estimation?

*Detection of  $BP_{ND}$  change with dual injections*

The MI-SRTM assumes that  $BP_{ND}$  alters promptly from  $BP_{ND1}$  to  $BP_{ND2}$  at the time of the second injection and then remains constant. However, in reality this is unlikely and the binding condition of [<sup>11</sup>C]raclopride may be continuously changed along time. In this simulation, the detectability of the reduction of  $BP_{ND}$  due to changes in binding conditions was investigated. Noiseless time–activity curves of the striatum and cerebellum were generated with a measured plasma TAC and assumed parameter values derived from measurements taken from the monkey study. A TAC of the cerebellum was simulated with a conventional two-tissue compartment, four-parameter model with assumed parameter values obtained previously in our monkey study:  $K_1 = 0.034$ ,  $K_1/k_2 = 0.36$ ,  $k_3 = 0.022$ ,  $k_4 = 0.034$ . Meanwhile, a TAC of the striatum was simulated with an extended two-tissue compartment model

expressed as Eq. (3) by the fourth-order Runge–Kutta method (Endres et al., 1997).

$$\begin{aligned} \frac{dC_f}{dt} &= K_1 C_p(t) - (k_2 + k'_3(t)) C_f(t) + k_4 C_b(t) \\ \frac{dC_b}{dt} &= k'_3(t) C_f(t) - k_4 C_b(t) \\ k'_3(t) &= k_{on} \frac{B_{max} - C_b(t)}{1 + D(t)} \\ D(t) &= B_1 \quad (t < t_2) \\ &= B_2 + A \cdot \exp(-R(t - t_2)) \quad (t \geq t_2) \end{aligned} \quad (3)$$

where  $C_f$  and  $C_b$  are the concentrations of radioactivity for free and specifically bound [ $^{11}\text{C}$ ]raclopride in tissue, respectively;  $B_{max}$  is the total dopamine  $D_2$  receptor concentration;  $k_{on}$  is the bimolecular association rate constant for raclopride;  $SA$  is the specific activity of administered [ $^{11}\text{C}$ ]raclopride;  $D$  is the concentration of free dopamine. In this simulation study,  $t_2$  was set to 30 min, and  $SA$  that was decay corrected to the first injection time was assumed to be equal in first and second injections with a single synthesis. Each assumed parameter for  $K_1$  to  $k_4$  was obtained from our monkey study, and the  $B_{max}$  value was as reported previously (Endres et al., 1997), thus  $K_1 = 0.033$ ,  $K_1/k_2 = 0.59$ ,  $k_{on} = 0.0048$ ,  $B_{max} = 17.6$ ;  $k_4 = 0.026$ ;  $B_1 = B_2 = 0$ , and  $SA = 37 \text{ GBq}/\mu\text{mol}$  at the time of first injection.

First, the magnitude of the  $BP_{ND}$  change, derived from an increase in released dopamine, was investigated. Time–activity curves, including dopamine release, were simulated from Eq. (3), in which  $A$  varied: 0.5, 1.0, 1.5 and 2.0, and  $R$  varied: 0.04, 0.07, and 0.1. In these simulated TACs,  $BP_{ND1}$  and  $BP_{ND2}$  were estimated by the MI-SRTM, and the relationship between the magnitude of the BP reduction ( $\Delta BP = (BP_{ND1} - BP_{ND2})/BP_{ND1}$ ) and the integral of the dopamine pulse  $D$  in Eq. (3) was examined.

Next, the BP change caused by an increase in administered raclopride was investigated.  $D(t)$  in Eq. (3) was set to 0, and tissue TACs were generated using the input plasma TAC in which administration of the first injection was assumed as 1 nmol raclopride, and the second injection was amplified from 1 to 50 times greater than the first injection. In these simulated TACs,  $BP_{ND1}$  and  $BP_{ND2}$  were estimated by the MI-SRTM, and the relationship between the magnitude of  $\Delta BP$  and the amount of raclopride administered by the second injection was examined.

#### Effect of binding change timing on $BP_{ND}$ estimates

It is possible that the change in  $BP_{ND}$  occurs either before, or after, the second injection of [ $^{11}\text{C}$ ]raclopride. In the MI-SRTM, the error in the estimates for the first injection of [ $^{11}\text{C}$ ]raclopride amplifies the errors in the estimates for the second injection. In this simulation, the effect of the onset of the dopamine pulse on the binding change of  $BP_{ND}$ , estimated by the MI-SRTM, was investigated using noiseless simulated TACs. First, TACs with a released dopamine pulse were generated using Eq. (3), with the parameters mentioned above, and three types of pulse ( $A = 0.5$ ,  $R = 0.1$ ;  $A = 1.0$ ,  $R = 0.07$ ;  $A = 1.5$ ,  $R = 0.04$ ) in which the onset time of the dopamine pulse,  $t_2$  in Eq. (3), was changed from  $-10$ ,  $-5$ ,  $0$ ,  $5$ ,  $10$ ,  $15$  min against 30 min intervals of the second injection. The values for  $BP_{ND1}$ ,  $BP_{ND2}$ , and  $\Delta BP$  were estimated by the MI-SRTM, and the relationship between the onset time of the dopamine pulse and the  $BP_{ND}$  estimates was investigated.

Next, TACs were generated by the SRTM with measured cerebellum TACs and assumed parameter values ( $R_1 = 0.86$ ,  $k_2 = 0.091$ , and  $BP_{ND1} = 2.2$ ) using the fourth-order Runge–Kutta method, assuming a prompt change of  $BP_{ND}$  at  $-10$ ,  $-5$ ,  $0$ ,  $5$  and  $10$  min after the second injection (30 min intervals). The value of  $BP_{ND2}$  was also varied so that

$\Delta BP$  would be 0, 10, 20, 30, 40, 50, 60, 70, and 80%. In these simulated TACs,  $BP_{ND1}$ ,  $BP_{ND2}$ , and  $\Delta BP$  were estimated by the MI-SRTM, and the estimated values were compared with the true values.

#### Effect of injection interval on $BP_{ND}$ estimates

The relationship between the reliability of the  $BP_{ND}$  estimates from the MI-SRTM and the injection interval was investigated with noise-added TACs. A dynamic tracer concentration for [ $^{11}\text{C}$ ]raclopride was derived from the equation of MI-SRTM (Eq. (2)) with a measured cerebellum TAC used as the input function and the rate constant values given as true values ( $R_1 = 0.95$ ,  $k_2 = 0.067$ ,  $BP_{ND1} = 2.6$ ,  $BP_{ND2} = 2.6$ ,  $1.8$ , or  $0.78$ ) assuming a prompt BP reduction at the time of the second injection. The timing of the second injection was varied from 20 min to 90 min after the first scan.

The Gaussian-distributed mean-zero noise with variance proportional to the true count was added to the non-decaying tissue activity for each frame using Eq. (4) (Logan et al., 2001):

$$\sigma_i(\%) = 100 \cdot F / \sqrt{C_i(t_i) \cdot e^{-\lambda t_i} \cdot \Delta t_i} \quad (4)$$

where  $i$  is the frame number;  $C_i$  is the non-decaying tissue radioactivity concentration derived from the rate constants and the input function;  $t_i$  is the midpoint time of the  $i$ 'th frame;  $\Delta t_i$  is the data collection time;  $\lambda$  is the radioisotope decay constant;  $F$  is a scaling factor representing the sensitivity of the measurement system, introduced here to adjust the noise level. It should be noted that this equation assumes that noise, which is added to the TAC, is determined by the count of the curve itself. In fact, noise is determined by the total counts in the slice, and is affected by random counts, dead time, etc. In this simulation study,  $F$  was set to 15.0 so that the noise level would be the same as the noise level for regions of interest (ROI)-based analysis, and 1000 noisy data sets were generated for each injection interval.

In these simulated TACs,  $BP_{ND1}$  and  $BP_{ND2}$  were estimated by the MI-SRTM, and estimated  $BP_{ND1}$ ,  $BP_{ND2}$ , and  $\Delta BP$  values were compared with the true values. Parameter estimates were considered outliers if either  $BP_{ND1}$  or  $BP_{ND2}$  was outside the range  $0.0 < BP_{ND} < 10.0$ . The reliability of the estimated parameters was evaluated by the mean and coefficient of variation (COV;  $SD/\text{mean}[\%]$ ) of the estimates excluding outliers, and the relationship between the reliability of the parameter estimates and the injection interval was investigated.

#### Monkey study analysis

Studies on monkeys with dual injections of [ $^{11}\text{C}$ ]raclopride were performed to determine whether the present approach can estimate two identical  $BP_{ND}$  values when there is no change in binding conditions during the scan, and whether this approach can detect a change in  $BP_{ND}$  values when the binding conditions do change during the scan. The monkeys were maintained and handled in accordance with guidelines for animal research on Human Care and Use of Laboratory Animals (Rockville, National Institute of Health/Office for Protection from Research Risks, 1996). The study protocol was approved by the Subcommittee for Laboratory Animal Welfare of the National Cardiovascular Center.

First, PET studies were performed in four cynomolgus macaques (weight  $3.6 \pm 0.56 \text{ kg}$ ) by administering the same molar amount of [ $^{11}\text{C}$ ]raclopride for the first and second injections (Table 1). Anesthesia was induced with ketamine (8.4 mg/kg, intramuscularly) and xylazine (1.7 mg/kg, intramuscularly) and maintained by intravenous propofol (6 mg/kg/h) and vecuronium (0.02 mg/kg/h) during the scan. Initially,  $418 \pm 111 \text{ MBq}$  of [ $^{11}\text{C}$ ]raclopride was administered by a bolus injection, and after 30 min, the same molar amount of [ $^{11}\text{C}$ ]raclopride as for the first injection, was administered by a bolus

**Table 1**  
Injection protocol in monkey studies with dual injections of [<sup>11</sup>C]raclopride.

	Subject	Specific activity at the time of first injection [GBq/μmol]	Injection interval [min]	First injection		Second injection	
				Injected mass [nmol]	Injected activity at the time of first injection [MBq]	Injected mass [nmol]	Injected activity at the time of second injection [MBq]
Exp. 1	#1	64.9	30	8.4	548		198
	#2	75.2	30	5.9	444		160
	#3	29.3	30	13.6	399	Same as first injection	144
	#4	39.7	30	7.1	280		101
	mean ± SD	52.3 ± 21.4	30	8.8 ± 3.4	418 ± 111		151 ± 39.9
Exp. 2	#5	22.6	30	3.3	73.3	30.7	249

Exp. 1: Dual injections with same mass of [<sup>11</sup>C]raclopride.

Exp. 2: Dual injections with different mass of [<sup>11</sup>C]raclopride.

injection. Data were acquired for 60 min (10 s × 18, 30 s × 6, 120 s × 7, 300 s × 2 for the first injection; 10 s × 18, 30 s × 6, 120 s × 7, 300 s × 2 for the second injection). The specific radioactivity was 52.3 ± 21.4 GBq/μmol at the time of the first injection.

Next, PET studies were performed on a cynomolgus macaque (weight 6.0 kg) with the administration of different molar amounts of [<sup>11</sup>C]raclopride for the first and second injections by changing the volume of second injection with [<sup>11</sup>C]raclopride which was synthesized before the first injection (Table 1). For the first injection, a bolus of 73.3 MBq of [<sup>11</sup>C]raclopride, (3.3 nmol of raclopride) was administered, and after 30 min, 249 MBq at the time of the second injection (decay corrected 691MBq) of [<sup>11</sup>C]raclopride (30.7 nmol of raclopride) was administered by bolus injection. The specific radioactivity was 23 GBq/μmol at the time of the first injection.

PET scans were performed using a PCA-2000A positron scanner (Toshiba Medical Systems Corporation, Tochigi, JAPAN) that provides 47 planes and a 16.2 cm axial field of view. A transmission scan with a 3-rod source of <sup>68</sup>Ge–<sup>68</sup>Ga was carried out for 20 min for attenuation correction before the administration of [<sup>11</sup>C]raclopride. Radioactivity was measured in two-dimensional mode and the data were reconstructed by a filtered back-projection using a Gaussian filter (full width at half maximum is about 6.0 mm (Herzog et al., 2004)). VOIs were defined manually over the left and right striatum and cerebellum for PET images, and the radioactivity concentration in these regions was obtained. For each region,  $R_{11}$ ,  $k_{21}$ ,  $BP_{ND1}$ ,  $R_{12}$ ,  $k_{22}$ , and  $BP_{ND2}$  were estimated by MI-SRTM. In addition, parametric images were generated, estimating each parameter voxel by voxel, using the MI-SRTM with the basis function method.

## Results

### Detection of $BP_{ND}$ change with dual-injection

Typical examples of simulated TACs in the dual-injection study with dopamine release are shown in Fig. 1. In the simulation studies, the magnitude of  $\Delta BP$ , estimated by the MI-SRTM, was investigated in the two cases where the specific binding changed due to the released dopamine pulse or to an increase in administered raclopride. The magnitude of  $\Delta BP$  increased as the integral of the dopamine pulse increased (Fig. 2A). To some extent there was a good linear correlation between the reduction in  $BP_{ND}$  and the integral of the dopamine pulse ( $Y = 2.0 * X + 2.3$ ,  $R^2 = 0.95$  where  $X < 15$  ( $X$ : Integral of the dopamine pulse,  $Y$ : reduction in  $BP_{ND}$ )); however the relationship did not remain linear for a large dopamine pulse. The reduction in  $BP_{ND}$  also became greater when the injected mass of raclopride increased, although its relationship was nonlinear (Fig. 2B).

### Effect of binding change timing on $BP_{ND}$ estimates

In the simulation with a released dopamine pulse, when the dopamine pulse was released before the second injection, the  $BP_{ND1}$  value was underestimated and  $BP_{ND2}$  was overestimated, compared with the situation where the dopamine pulse was released at the same time as the second injection (Figs. 3A, B). On the other hand, when the dopamine pulse was released after the second injection,  $BP_{ND1}$  was unchanged and  $BP_{ND2}$  varied according to the onset and magnitude of the dopamine pulse. The reduction in  $BP_{ND}$  also depended on the

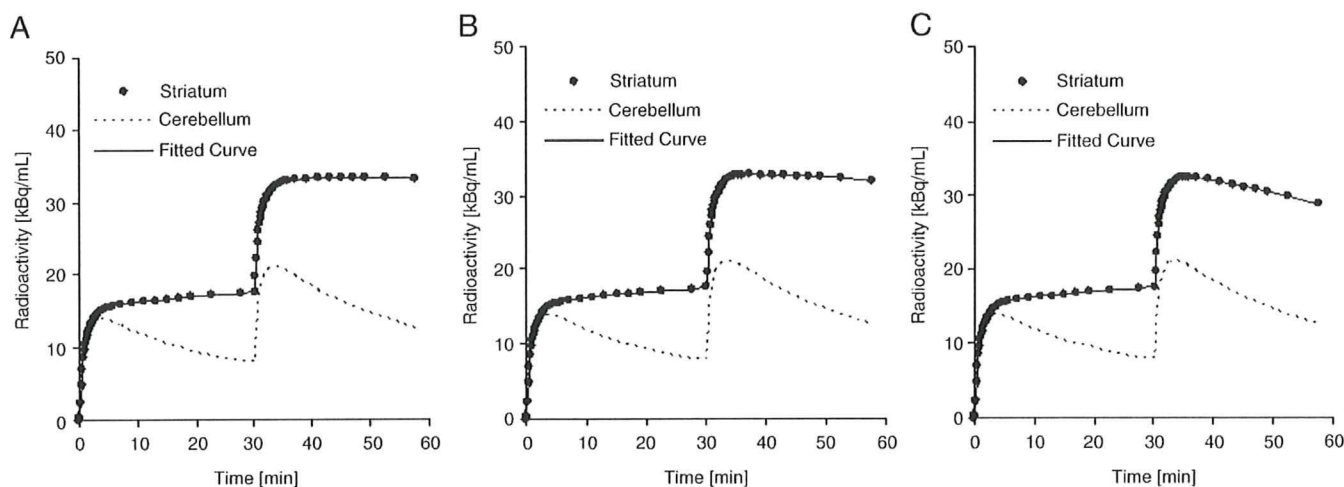


**Fig. 1.** Simulated time-activity curves for the striatum and cerebellum without dopamine pulse (A), with small dopamine pulse ( $A = 0.5$ ,  $R = 0.04$ ) (B), and with large dopamine pulse ( $A = 1.5$ ,  $R = 0.1$ ) (C), and fitted curve for the striatum by MI-SRTM.

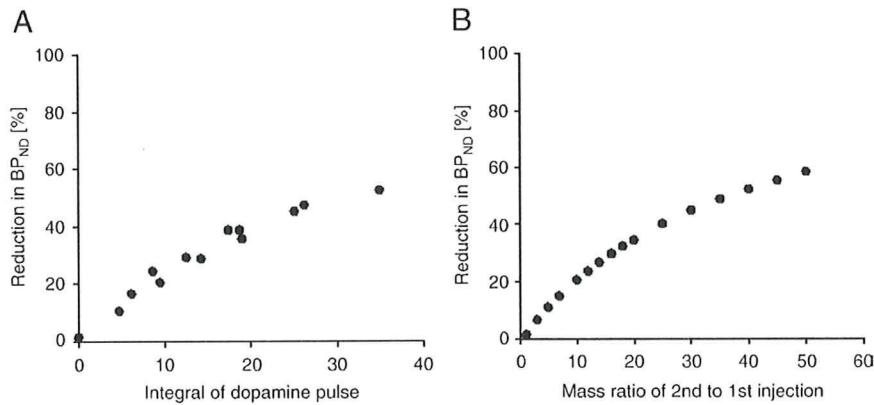


Fig. 2. Relationship between percentage reduction in BP<sub>ND</sub> and the integral of the dopamine pulse in simulation studies in which dopamine was released at the same time as the second injection, performed 30 min after first injection (A); and the relationship between percentage reduction in BP<sub>ND</sub> and the mass of the second injection in simulation studies in which a greater mass of raclopride was administered 30 min after the first injection.

onset, magnitude of amplitude, and decay rate of the dopamine pulse, and the reduction in BP<sub>ND</sub> was greatest when the dopamine pulse was released 5 min after the second injection (Fig. 3C). When the magnitude of the dopamine pulse was small, the detected BP<sub>ND</sub> reduction was small when the dopamine pulse was released before the second injection, becoming greatest (about 20%) when the pulse was released 5 min or 10 min after the second injection. When the magnitude of the pulse was medium, the BP<sub>ND</sub> reduction was 20% when the pulse was released 5 min before the second injection, and it was greatest (about 35%) when the pulse was released 5 min after the second injection. When the dopamine pulse was large, the detected BP<sub>ND</sub> reduction was 30% even when the pulse was released 10 min before the second injection, and was greatest (about 45%) when the pulse was released 0 or 5 min after the second injection.

In the simulation with prompt BP<sub>ND</sub> reduction, BP<sub>ND1</sub>, BP<sub>ND2</sub> and  $\Delta$ BP were estimated precisely by the MI-SRTM when the BP<sub>ND</sub> reduction occurred at 30 min, in other words, at the same time as the second injection (Fig. 4). In the case where the BP decreased before 30 min, the estimated BP<sub>ND1</sub> was lower than the true value for BP<sub>ND1</sub> (=2.2), and the magnitude of the underestimation increased when the true BP<sub>ND2</sub> was lower, that is to say, the reduction in BP<sub>ND</sub> was greater (Fig. 4A). There were slight errors in BP<sub>ND2</sub> estimates (Fig. 4B). When the BP<sub>ND</sub> decreased 50% (BP<sub>ND1</sub> = 2.2 and BP<sub>ND2</sub> = 1.1) at 10 min before the second injection, estimated BP<sub>ND1</sub> was 1.63 and BP<sub>ND2</sub> was 1.04. Conversely, when the BP decreased after 30 min, BP<sub>ND1</sub> was estimated precisely, and BP<sub>ND2</sub> was overestimated (Figs. 4A and B). The error in BP<sub>ND2</sub> estimates increased as the magnitude of the

BP<sub>ND</sub> reduction increased. When the BP<sub>ND</sub> decreased 50% (BP<sub>ND1</sub> = 2.2 and BP<sub>ND2</sub> = 1.1) at 10 min after the second injection, estimated BP<sub>ND1</sub> was 2.20 and BP<sub>ND2</sub> was 1.28. With respect to the magnitude of the BP reduction, the estimated  $\Delta$ BP was lower than the true value when the BP reduction was greater, or the difference between the timing of the BP<sub>ND</sub> decrease and the second injection was greater (Fig. 4C). When the BP<sub>ND</sub> reduction began 10 min before the second injection, the error in the estimated  $\Delta$ BP was considerable. However, when the BP<sub>ND</sub> reduction began, either 5 min before or 5 min after, the second injection, the error in  $\Delta$ BP was less than 5% when the reduction in the BP was lower than 50%.

#### Effect of injection interval on BP<sub>ND</sub> estimates

Errors in the estimated BP<sub>ND1</sub>, BP<sub>ND2</sub> and  $\Delta$ BP values were investigated in simulated noise-added TACs for various injection intervals, and it was observed that the errors became larger as the injection interval became shorter (Fig. 5). The COVs of BP<sub>ND1</sub> and BP<sub>ND2</sub> were less than 5% and the bias was less than 1% when the injection interval was longer than 30 min, in both cases where the reduction in the BP<sub>ND</sub> was 30% and 70%. When  $\Delta$ BP was 30%, the bias increased suddenly, and the COV of  $\Delta$ BP rose to over 10% for an injection interval of less than 40 min. There were no outliers even if the injection interval was 20 min. Meanwhile, when  $\Delta$ BP was 70%, there was little bias and the COV of  $\Delta$ BP was less than 10% for an injection interval longer than 30 min. The COV of  $\Delta$ BP in the 70% reduction TAC was lower than that in 30% reduction TAC. However,

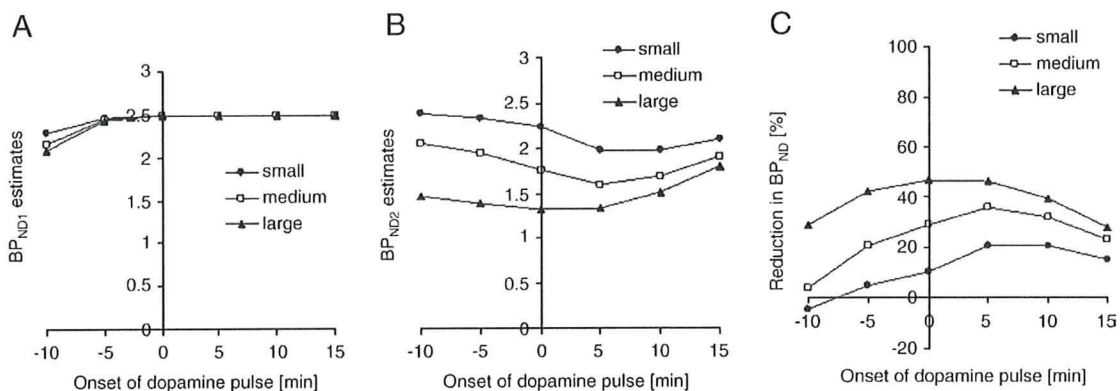


Fig. 3. Relationship between estimated values of BP<sub>ND1</sub> (A), BP<sub>ND2</sub> (B), reduction in BP<sub>ND</sub> (C) and the onset of the dopamine pulse, in simulation studies with a small pulse ( $H=0.5$ ,  $R=0.1$ ), medium pulse ( $H=1.0$ ,  $R=0.07$ ), and large pulse ( $H=1.5$ ,  $R=0.04$ ) released  $-10$ ,  $-5$ ,  $0$ ,  $+5$ ,  $+10$ , or  $+15$  min with respect to the second injection.

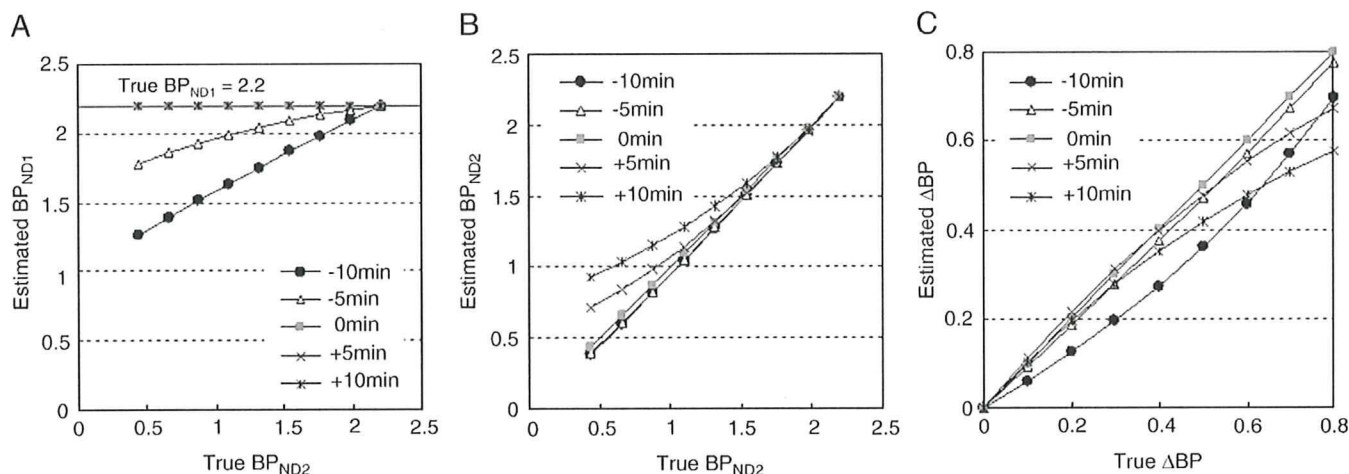


Fig. 4. Relationship between estimated values of  $BP_{ND1}$  (A), and  $BP_{ND2}$  (B) and the true values of  $BP_{ND2}$ , and the relationship between the estimated reduction in  $BP_{ND}$  ( $\Delta BP$ ) and true  $\Delta BP$  (C) in the simulation studies in which  $BP_{ND}$  changed promptly from 2.2 to the true  $BP_{ND2}$  at -10, -5, 0, +5, or +10 min, with respect to the second injection.

there were 22 outliers with unreasonable estimates when the injection interval was 20 min and one outlier in one thousand estimates when the injection interval was 30 min.

Monkey studies

Typical examples of TACs for the striatum and the cerebellum in the dual-injection study with the same amount of raclopride are

shown in Fig. 6. In these studies, the  $BP_{ND}$  values for the first and second injections could be estimated, and there were little differences between  $BP_{ND1}$  and  $BP_{ND2}$  (Table 2).

Time-activity curves for the striatum and the cerebellum in the dual-injection study using different amounts of raclopride are shown in Fig. 7, and the parametric images of  $BP_{ND1}$  and  $BP_{ND2}$  are shown in Fig. 8. The estimated BP decreased when the binding changed at the second injection due to the addition of more raclopride than was

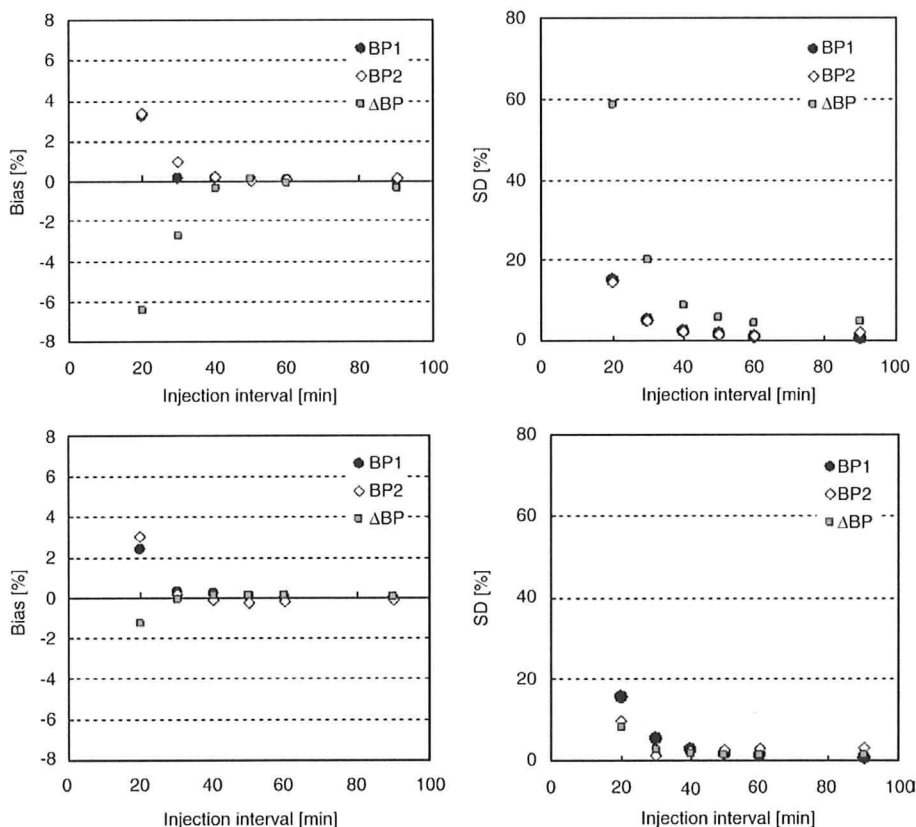
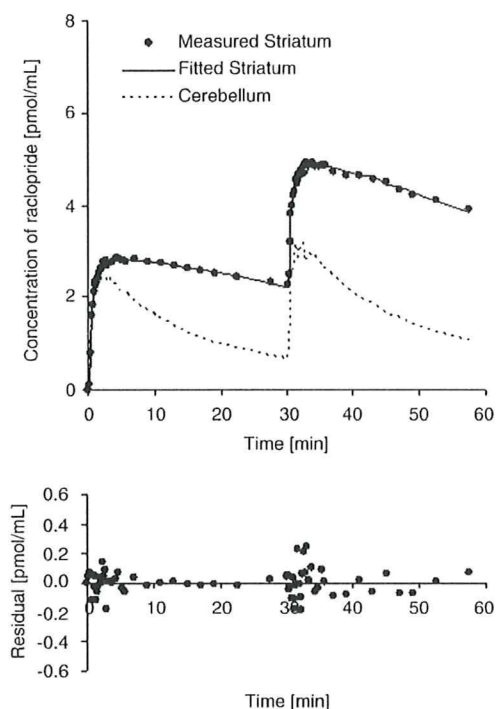


Fig. 5. Relationship between the injection interval and bias (left) or SD (right) of  $BP_{ND1}$ ,  $BP_{ND2}$ , and the reduction in  $BP_{ND}$  ( $\Delta BP$ ) when  $BP_{ND}$  decreased by 30% (upper) or 70% (lower) at the time of second injection.



**Fig. 6.** Measured time-activity curves of the striatum and cerebellum in the dual-injection study with the same mass of [ $^{11}\text{C}$ ]raclopride and a fitted curve for the striatum, using the multiple-injection SRTM (upper), and residuals between measured and fitted curves (lower).

administered for the first injection. Estimated  $\text{BP}_{\text{ND}1}$ ,  $\text{BP}_{\text{ND}2}$  and  $\Delta\text{BP}$  values in the striatum were 2.7, 2.0, and 25%, respectively (Table 2). The reduction in  $\text{BP}_{\text{ND}}$  was also observed in the parametric images as shown in Fig. 8.

## Discussion

In the competition paradigm, the binding potential of [ $^{11}\text{C}$ ]raclopride reflects the condition of specific binding to dopamine  $\text{D}_2$  receptors, which is affected by competition with other ligands if there are no changes in the density of the receptors. The SRTM can provide the  $\text{BP}_{\text{ND}}$  value without invasive arterial blood sampling, using a TAC of the reference region, where specific bindings are negligible (Lammertsma and Hume, 1996), and this method has been widely used to estimate the binding of neuroreceptor ligands. However, in assessing temporal changes in the  $\text{BP}_{\text{ND}}$  of the SRTM caused by competition for receptor binding due to pharmacological administration or cognitive activation, multiple [ $^{11}\text{C}$ ]raclopride PET scans are necessary and a long study period is required. To overcome this complication, we have proposed a multiple-injection approach in which the temporal change in  $\text{BP}_{\text{ND}}$  is quantified in a single scan with multiple [ $^{11}\text{C}$ ]raclopride

**Table 2**

Estimated  $\text{BP}_{\text{ND}1}$ ,  $\text{BP}_{\text{ND}2}$ , and difference between  $\text{BP}_{\text{ND}1}$  and  $\text{BP}_{\text{ND}2}$  in monkey studies with dual injections of [ $^{11}\text{C}$ ]raclopride.

	Subject	$\text{BP}_{\text{ND}1}$	$\text{BP}_{\text{ND}2}$	$\Delta\text{BP}$
Exp. 1	#1	1.86	2.15	0.15
	#2	1.98	2.01	0.014
	#3	1.95	1.79	-0.081
	#4	2.33	2.39	0.027
	mean $\pm$ SD	$2.03 \pm 0.20$	$2.08 \pm 0.25$	$0.029 \pm 0.097$
Exp. 2	#5	2.66	2.00	-0.25

$\Delta\text{BP} = (\text{BP}_{\text{ND}2} - \text{BP}_{\text{ND}1}) / \text{BP}_{\text{ND}1}$ .

Exp. 1: Dual injections with same mass of [ $^{11}\text{C}$ ]raclopride.

Exp. 2: Dual injections with different mass of [ $^{11}\text{C}$ ]raclopride.

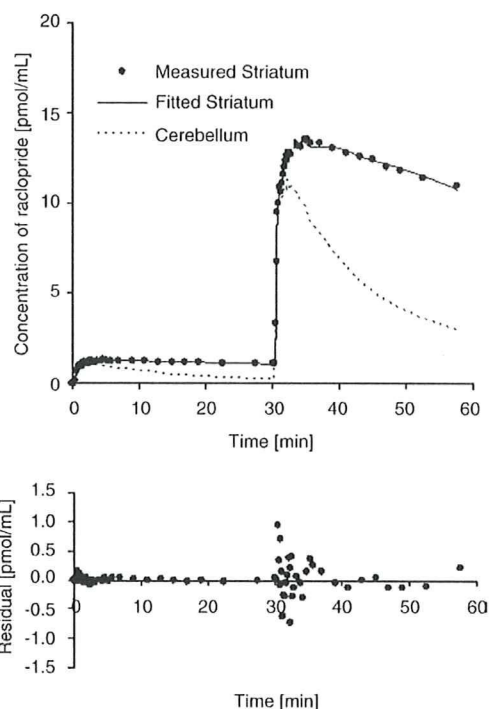


**Fig. 7.** Measured time-activity curves of the striatum and cerebellum in the dual-injection study with a different mass of [ $^{11}\text{C}$ ]raclopride and a fitted curve for the striatum, using the multiple-injection SRTM (upper), and residuals between measured and fitted curves (lower).

injections. This approach takes into account the residual radioactivity from the first injection in the target tissue, at the time of the second injection, as the initial condition in Eq. (2), and makes it possible to perform the second injection immediately, following data acquisition from the first injection. Thus it is possible to determine the change in  $\text{BP}_{\text{ND}}$  from a short study period.

There have been several investigators who attempted to perform multiple injections of ligands with PET studies for either obtaining receptor density and affinity by changing specific activity (Delforge et al., 1995; Millet et al., 1995; Morris et al., 1996a,b; Muzic et al., 1996; Christian et al., 2004; Gallezot et al., 2008), or obtaining different kinetic parameters simultaneously by injecting different tracers such as [ $^{11}\text{C}$ ]flumazenil and [ $^{18}\text{F}$ ]FDG (Ikoma et al., 2004; Koeppe et al., 2001). MI-SRTM gives us alternative approach for multiple-injection study which is aimed at shortening study period.

### Detection of binding changes with the SRTM

In the multiple-injection approach, it is assumed that the change in binding conditions is reflected by a reduction in  $\text{BP}_{\text{ND}}$  estimated from the SRTM. The analysis method based on the compartment model assumes that the rate constants of  $K_1$  to  $k_4$  are constant during the scan. However, in studies with changes in binding conditions, levels of endogenous dopamine change after exposure to stimuli such as an amphetamine challenge (Endres et al., 1997; Laruelle et al., 1997), and the value of  $k_3'(t)$  in Eq. (3) varies according to the concentration of free dopamine (Laruelle et al., 1997; Endres et al., 1997). Therefore, estimates of  $\text{BP}_{\text{ND}}$  following exposure to stimuli are considered to be an average value over time that is influenced by the dynamics of the neurotransmitter. However, it has been reported that reductions in  $\text{BP}_{\text{ND}}$ , estimated from graphical analysis or multilinear analysis, in simulation studies for two separate bolus-injection scans, are related to the integral of dopamine release (Endres and Carson, 1998; Yoder et al., 2004), and the reduction in  $\text{BP}_{\text{ND}}$  is a useful index for the evaluation of binding conditions in competition paradigms.

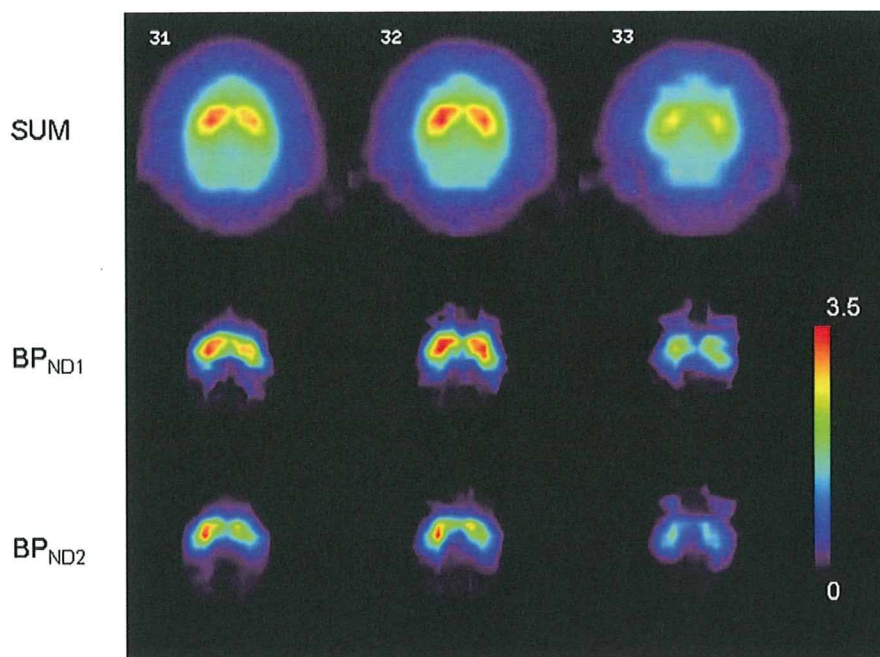


Fig. 8. Summation image and parametric images of  $BP_{ND1}$  and  $BP_{ND2}$  in the monkey study with dual injections of different masses of [ $^{11}C$ ]raclopride.

In addition, in the SRTM, there are further assumptions that the target tissue and reference tissue can be expressed by a one-tissue compartment model, and the ratio of  $K_1$  and  $k_2$  are equal between the target and reference regions (Lammertsma and Hume, 1996). Strictly speaking, this assumption does not apply to [ $^{11}C$ ]raclopride studies because significantly better fits were obtained with a two-tissue compartment model, as compared with those obtained with a one-tissue compartment model in cerebellum and striatum TACs (Lammertsma et al., 1996). Therefore, this assumption of the SRTM induces a bias in  $BP_{ND}$  estimates even in an ordinary single-injection study. In the MI-SRTM, which is an extension of the SRTM, the effect of the assumption could be more severe than for the SRTM because the bias in  $BP_{ND1}$  could be propagated to the estimation of  $BP_{ND2}$ . However, in our simulation studies, the  $\Delta BP_{ND}$ , estimated from the MI-SRTM, increased according to the increase in the dopamine pulse or to administered raclopride (Fig. 2). When the specific binding of administered [ $^{11}C$ ]raclopride competed with that of endogenous dopamine, to some extent the reduction in BP increased in proportion to the integral of the released dopamine pulse, and approached saturation as the integral of the pulse increased. This is consistent with results reported in previous studies (Endres and Carson, 1998, Yoder et al., 2004). Furthermore, in the monkey studies, it was confirmed that there was little change in  $BP_{ND}$  when the same mass of raclopride was administered for the first and second injections (Fig. 6), and the  $BP_{ND}$  decreased in accordance with the increase in administered raclopride (Figs. 7 and 8). Morris et al. (1996b) intensively investigated the characteristics of multiple injections PET studies, and they showed varied specific activity by multiple injections introduced bias in estimates of kinetic parameters. Our results may be influenced by the abrupt discontinuity in mass of raclopride due to the second injection. However, the result of second monkey study (10 times higher mass in the second injection) agreed well with the simulation (Fig. 2B) although further validation studies will be needed to confirm this result.

#### Effect of binding change timing on $BP_{ND}$ estimates

In estimating the  $BP_{ND}$  after the dopamine pulse release, the timing of the [ $^{11}C$ ]raclopride injection has been shown to affect the  $BP_{ND}$  estimates (Yoder et al., 2004). In the simulation study of our multiple-

injection approach,  $BP_{ND1}$  (in other words, the  $BP_{ND}$  for the condition without dopamine activation) had few errors, except when the dopamine pulse was released 10 min before the second injection. In these simulations,  $BP_{ND1}$  was estimated using the data from the time interval between the first injection and the second injection. Therefore, when the  $BP_{ND}$  reduction, due to an increase in free dopamine, started before the second injection, the value for  $BP_{ND1}$  was underestimated. However, this underestimation can be avoided by adjusting the data points used for the fitting of  $BP_{ND1}$  so that  $BP_{ND1}$  is determined before a change in the binding conditions. On the other hand,  $BP_{ND2}$ , (that is to say, the  $BP_{ND}$  of the condition with dopamine activation) was affected by the timing of the dopamine pulse release. The estimated  $BP_{ND2}$  decreased as the onset of the dopamine pulse occurred later, and was smallest when the dopamine pulse was released 5 min after the second injection. As a result, the magnitude of  $\Delta BP$  was greatest when the dopamine pulse was released 5 min after the second injection.

The value of  $k_3^*(t)$  in Eq. (3) depends upon the amount of free dopamine at time  $t$  (Endres et al., 1997, Endres and Carson, 1998) and the released dopamine pulse decreases as time goes by. Therefore, if the specific activity of administered [ $^{11}C$ ]raclopride is high enough, the time-varying binding potential ( $BP_s(t) = k_3^*(t)/k_4$ ) is lowest at the time of the pulse release, and it becomes greater, and approaches the level before the pulse release, as time passes. Meanwhile, the reduction in  $BP_{ND}$  is determined by both the  $BP_s(t)$  and the concentration of free tracer (Endres and Carson, 1998). In the TACs from our simulation studies, the concentration of free [ $^{11}C$ ]raclopride had a peak at about 5 min after the injection, and  $\Delta BP_{ND}$  was greatest when the onset of the dopamine pulse occurred 5 min after the injection, as shown in Fig. 3C. Therefore, the reduction in  $BP_{ND}$  was greatly affected, not only by the magnitude of the dopamine pulse, but also by its timing. In other words, if the kinetics of the free tracer are similar, that is to say the value of  $k_2$  does not change markedly, and the timing of the dopamine release is the same, the estimated  $\Delta BP$  changes according to the integral of the dopamine pulse as shown in Fig. 2.

In the situation where  $BP_{ND}$  changed promptly, the  $\Delta BP_{ND}$  also depends upon the magnitude and timing of the  $BP_{ND}$  reduction. However, when  $\Delta BP_{ND}$  was less than 40% and the time difference

between the binding change and second injection was within 5 min, the effect of the timing of the  $BP_{ND}$  reduction was slight.

#### *Interval between the dual injections*

In the simulation study with noise for the ROI-based estimation, a dual-injection scan with a 30 min injection interval, gave unbiased and reliable  $BP_{ND1}$  and  $BP_{ND2}$  estimates (Fig. 5). In the 70% reduction TAC, the COV of  $\Delta BP_{ND}$  was less than 5% when the injection interval was 30 min. Conversely, results from the 30% reduction TAC showed that a 50 min interval would be required to estimate  $\Delta BP_{ND}$  within a 5% COV. In this study, we evaluated the reliability of  $BP_{ND}$  estimates for an ROI-based estimation. However, in voxel-based estimations, the noise level is usually higher, so the COV of estimates can be expected to increase.

In the ROI analysis of human study with single injection, it is reported that a 30 min scan of [ $^{11}C$ ]raclopride gave unbiased and reliable  $BP_{ND}$  estimates (Ikoma et al., 2008). The kinetics of [ $^{11}C$ ]raclopride in the human brain is different from that in the monkey brain, inducing the difference in required scan durations. The required injection interval for a reliable estimation depends on the kinetics of the ligand, the magnitude of  $\Delta BP_{ND}$  and the noise level according to injection dose, ROI size, sensitivity of the measurement system, and so on. Therefore, evaluating the effect of the injection interval on the reliability of parameter estimates is important.

#### *Monkey studies*

In the simulation studies, it was demonstrated that the MI-SRTM approach could detect a change in  $BP_{ND}$  caused by the release of a dopamine pulse or by the increase in administered raclopride. Furthermore, we demonstrated the validity of the proposed method using actual data from monkeys. As a result, the estimated  $BP_{ND}$  reduction changed according to the injected mass of raclopride in the second injection, and this is consistent with the results from the simulation studies. We are planning further studies on monkeys with co-injection of various amount of cold raclopride to examine the relationship between the observed changes in  $BP_{ND}$  and the occupancy of receptors. Furthermore, using the present approach, it may be possible to estimate endogenous dopamine release by pharmaceutical stimuli although the interpretation of the results must be made with caution because the level of endogenous dopamine is sensitive to the timing and the response of pharmaceutical manipulation (Yoder et al., 2004).

#### *Potential of the multiple-injection approach*

The dual-injection approach is able to assess the change in  $BP_{ND}$  for receptor competition studies in a single PET scan and shortened study period, as compared to a conventional approach. However, this approach requires some caution. Firstly, the error due to residual radioactivity at the time of the second injection may affect the reliability of  $BP_{ND2}$  estimates. Therefore, we estimated the residual radioactivity, not from the measured TAC, but from a fitted TAC from the first injection. In the simulation study, with noise-added TACs, the bias and COV of  $BP_{ND2}$  estimated from the second injection were acceptable (Fig. 5).

Secondly, the administered molar amount of second injection must be same as that of the first injection for the evaluation of dopamine release, because the value of  $BP_{ND}$  decreases according to the increase in administered raclopride even if the dopamine pulse does not be released (Fig. 2B). In addition, in the dual-injection study, the radioligand for the first injection remains in the tissue at the time of second injection. Therefore, the molar amount of administered raclopride needs to be sufficiently small, that is to say, the specific activity of administered [ $^{11}C$ ]raclopride should be high enough. The

mass of first injection is required to be less than about 1 nmol/kg so that the remained raclopride at the second injection does not affect  $BP_{ND2}$  estimates (data not shown). To keep the amount of administered raclopride below 1 nmol/kg with the administration of 37MBq/kg [ $^{11}C$ ]raclopride, its specific activity should be greater than 37 GBq/ $\mu$ mol. However, in the multiple-injection study, if one can synthesize [ $^{11}C$ ]raclopride with high specific activity, it is an advantage that [ $^{11}C$ ]raclopride, synthesized once before the scan, can be administered for both the first and second injections.

Thirdly, the timing of the second injection affected the  $BP_{ND}$  estimates, as it was also observed in the estimations using two separate conventional scans. The timing of the second injection should be fixed within the intersubjects of the group, and the interpretation of the  $\Delta BP_{ND}$  requires some caution when a time–activity curve of free [ $^{11}C$ ]raclopride differs. The competition paradigm also should be applied carefully in case where the dopamine released slowly in response to stimuli, because it is often difficult to estimate the timing of the dopamine peak. Despite this, we have shown that the multiple-injection approach can be used to determine a reduction in  $BP_{ND}$  values as effectively as using two separate scans, but within a single scan lasting 100 min.

The ESRTM approach can also provide  $\Delta BP_{ND}$  values from a single-session scan by administering [ $^{11}C$ ]raclopride using a bolus-plus-continuous (B/I) infusion approach (Zhou et al., 2006). Meanwhile, with the MI-SRTM approach, [ $^{11}C$ ]raclopride can be administered several times by bolus injection, so there is no need to control the administered dose continuously, and it is easy to change the administered mass of raclopride significantly during the scan.

Since the MI-SRTM is a successor of SRTM, one advantage of the MI-SRTM is that the  $BP_{ND}$  parametric map can be obtained as shown in Fig. 8, which is crucial to perform statistical parametric mapping (SPM) type analysis. The results of our simulation and monkey studies suggest that the MI-SRTM can be applied to the estimation of  $\Delta BP_{ND}$  for human study, though the optimal injection protocol needs to be evaluated. One application of the MI-SRTM approach for the human study is to estimate occupancy within short period. By the MI-SRTM approach, one can estimate the  $BP_{ND}$  value without antipsychotics and  $BP_{ND}$  with antipsychotics from one session of PET study. This approach is also useful in the estimation of receptor density ( $B_{max}$ ) and affinity ( $K_d$ ) that normally requires several scans with variable masses of raclopride injections (Farde et al., 1986; Doudet et al., 2003). Furthermore, this approach can be applied to other PET ligands if the  $BP_{ND}$  can be estimated by the SRTM approach.

In summary, we have developed a method for estimating the change in binding potential in a single PET scan using multiple injections of [ $^{11}C$ ]raclopride and a simplified reference tissue model. Our simulations showed that the reduction in  $BP_{ND}$ , estimated by this approach, was related to the amount of released dopamine or to the administered mass of raclopride. We also demonstrated that the reduction in  $BP_{ND}$  varied according to the increase in administered raclopride in monkey studies. The proposed method, with multiple injections, has potential for use in quantitatively assessing the change in specific binding, in a short study period, for several neurotransmitter competition studies.

#### **Acknowledgments**

This research was supported by the Ministry of Education, Culture, Sports, Science and Technology, Grant-in-Aid for Young Scientists (B) (No.20790839), Japan, Kobe Cluster I and II, Ministry of Education, Culture, Sports, Science and Technology of Japan (MEXT; T.H.), and the MHLW (Ministry of Health, Labour and Welfare of Japan) Health Science Research Grant, H17-025 (T.H., H.I.).

We are grateful to members of the Department of Investigative Radiology, National Cardiovascular Center Research Institute, for their support of the PET experiment and for helpful suggestions.

Appendix A

The multiple-injection simplified reference tissue model is based on the following differential equations of the simplified reference tissue model on the assumption that the time–activity curves of the target and reference tissues can be fitted to a single tissue compartment model with plasma input (Lammertsma and Hume, 1996)

$$\frac{dC_t}{dt} = K_1 C_p(t) - k_{2a} C_t(t) \tag{A1}$$

$$\frac{dC_r}{dt} = K_1^r C_p(t) - k_2^r C_r(t) \tag{A2}$$

$$K_1 / k_{2a} = K_1 / k_2 \cdot (1 + BP_{ND}) \tag{A3}$$

where  $C_p$  is the metabolite corrected plasma concentration,  $C_t$  and  $C_r$  are the concentration in target and reference tissue, respectively,  $k_{2a}$  ( $\text{min}^{-1}$ ) is the apparent (overall) rate constant for transfer from specific compartment to plasma in the target tissue.

Eqs. (A1) and (A2) are expressed as follows by Laplace transform:

$$sC_t(s) - C_t(0) = K_1 C_p(s) - k_{2a} C_t(s) \tag{A4}$$

$$sC_r(s) - C_r(0) = K_1^r C_p(s) - k_2^r C_r(s) \tag{A5}$$

where  $C_t(0)$  and  $C_r(0)$  are the total concentration in target and reference tissue, respectively, at the time of injection.

From Eqs. (A4),(A5) and the assumption  $K_1^r / k_2^r = K_1 / k_2$ , the following expression can be derived:

$$C_t(s) = R_1 C_r(s) + \frac{1}{s + k_{2a}} (k_2 - Rk_{2a}) C_r(s) + \frac{1}{s + k_{2a}} (C_t(0) - R_1 C_r(0)). \tag{A6}$$

From Eqs. (A3) and (A6), the following expression can be derived by inverse-Laplace transform:

$$C_t(t) = R_1 C_r(t) + \left( k_2 - \frac{R_1 k_2}{1 + BP_{ND}} \right) e^{-\frac{k_2}{1 + BP_{ND}} t} \otimes C_r(t) + (C_t(0) - R_1 C_r(0)) e^{-\frac{k_2}{1 + BP_{ND}} t}. \tag{A7}$$

In the second injection,  $R_1$ ,  $k_2$ , and  $BP_{ND}$  can be estimated by giving  $C_t(t)$ ,  $C_r(t)$ , and  $C_t(0)$  and  $C_r(0)$  at the time of second injection. Meanwhile, in the first injection,  $C_t(0)$  and  $C_r(0)$  are 0 at the time of first injection, so  $C_t(t)$  can be expressed as follows:

$$C_t(t) = R_1 C_r(t) + \left( k_2 - \frac{R_1 k_2}{1 + BP_{ND}} \right) e^{-\frac{k_2}{1 + BP_{ND}} t} \otimes C_r(t). \tag{A8}$$

References

Breier, A., Su, T.P., Saunders, R., Carson, R.E., Kolachana, B.S., de Bartolomeis, A., Weinberger, D.R., Weisenfeld, N., Malhotra, A.K., Eckelman, W.C., Pickar, D., 1997. Schizophrenia is associated with elevated amphetamine-induced synaptic dopamine concentrations: evidence from a novel positron emission tomography method. *Proc. Natl. Acad. Sci. U.S.A.* 94, 2569–2574.

Carson, R.E., Breier, A., de Bartolomeis, A., Saunders, R.C., Su, T.P., Schmall, B., Der, M.G., Pickar, D., Eckelman, W.C., 1997. Quantification of amphetamine-induced changes in [<sup>11</sup>C]raclopride binding with continuous infusion. *J. Cereb. Blood Flow Metab.* 17, 437–447.

Christian, B.T., Narayanan, T., Shi, B., Morris, E.D., Mantil, J., Mukherjee, J., 2004. Measuring the in vivo binding parameters of [18F]-fallypride in monkeys using a PET multiple-injection protocol. *J. Cereb. Blood Flow Metab.* 24, 309–322.

Delforge, J., Pappata, S., Millet, P., Samson, Y., Bendriem, B., Jobert, A., Crouzel, C., Syrota, A., 1995. Quantification of benzodiazepine receptors in human brain using PET, [<sup>11</sup>C] flumazenil, and a single-experiment protocol. *J. Cereb. Blood Flow Metab.* 15, 284–300.

Doudet, D.J., Jivan, S., Holden, J.E., 2003. In vivo measurement of receptor density and affinity: comparison of the routine sequential method with a nonsequential

method in studies of dopamine D<sub>2</sub> receptors with [<sup>11</sup>C]raclopride. *J. Cereb. Blood Flow Metab.* 23, 280–284.

Endres, C.J., Kolachana, B.S., Saunders, R.C., Su, T., Weinberger, D., Breier, A., Eckelman, W.C., Carson, R.E., 1997. Kinetic modeling of [<sup>11</sup>C]raclopride: combined PET-microdialysis studies. *J. Cereb. Blood Flow Metab.* 17, 932–942.

Endres, C.J., Carson, R.E., 1998. Assessment of dynamic neurotransmitter changes with bolus or infusion delivery of neuroreceptor ligands. *J. Cereb. Blood Flow Metab.* 18, 1196–1210.

Farde, L., Ehrin, E., Eriksson, L., Greitz, T., Hall, H., Hedstrom, C.G., Litton, J.E., Sedvall, G., et al., 1985. Substituted benzamides as ligands for visualization of dopamine receptor binding in the human brain by positron emission tomography. *Proc. Natl. Acad. Sci. U.S.A.* 82, 3863–3867.

Farde, L., Hall, H., Ehrin, E., Sedvall, G., 1986. Quantitative analysis of D<sub>2</sub> dopamine receptor binding in the living human brain by PET. *Science* 231, 258–261.

Gallezot, J.D., Bottlaender, M.A., Delforge, J., Valette, H., Saba, W., Dollé, F., Coulon, C.M., Ottaviani, M.P., Hinnen, F., Syrota, A., Grégoire, M.C., 2008. Quantification of cerebral nicotinic acetylcholine receptors by PET using 2-[<sup>18</sup>F]fluoro-A-85380 and the multiinjection approach. *J. Cereb. Blood Flow Metab.* 28, 172–189.

Gunn, R.N., Lammertsma, A.A., Hume, S.P., Cunningham, V.J., 1997. Parametric imaging of ligand–receptor binding in PET using a simplified reference region model. *Neuroimage* 6, 279–287.

Hall, H., Köhler, C., Gawell, L., Farde, L., Sedvall, G., 1988. Raclopride, a new selective ligand for the dopamine-D<sub>2</sub> receptors. *Prog. Neuropsychopharmacol. Biol. Psychiatry* 12, 559–568.

Herzog, H., Tellmann, L., Hocke, C., Pietrzyk, U., Casey, M.E., Kuwert, T., 2004. NEMA NU2-2001 guided performance evaluation of four Siemens ECAT PET scanners. *IEEE Trans. on Nucl. Science* 51, 2662–2669.

Ikoma, Y., Toyama, H., Suhara, T., 2004. Simultaneous quantification of two brain functions with dual tracer injection in PET dynamic study. In: Iida, H., Shah, N.J., Hayashi, T., Watabe, H. (Eds.), *Quantitation in Biomedical Imaging with PET and MRI*. InElsevier, pp. 74–78.

Ikoma, Y., Ito, H., Arakawa, R., Okumura, M., Seki, C., Shidahara, M., Takahashi, H., Kimura, Y., Kanno, I., Suhara, T., 2008. Error analysis for PET measurement of dopamine D<sub>2</sub> receptor occupancy by antipsychotics with [<sup>11</sup>C]raclopride and [<sup>11</sup>C] FLB457. *Neuroimage* 42, 1285–1294.

Kim, K.M., Watabe, H., Hayashi, T., Hayashida, K., Katafuchi, T., Enomoto, N., Ogura, T., Shidahara, M., Takikawa, S., Eberl, S., Nakazawa, M., Iida, H., 2006. Quantitative mapping of basal and vasoreactive cerebral blood flow using split-dose <sup>123</sup>I-iodoamphetamine and single photon emission computed tomography. *Neuroimage* 33, 1126–1135.

Koepp, M.J., Gunn, R.N., Lawrence, A.D., Cunningham, V.J., Dagher, A., Jones, T., Brooks, D.J., Bench, C.J., Grasby, P.M., 1998. Evidence for striatal dopamine release during a video game. *Nature* 393, 266–268.

Koepp, R.A., Raffel, D.M., Snyder, S.E., Ficano, E.P., Kilbourn, M.R., Kuhl, D.E., 2001. Dual-[<sup>11</sup>C]tracer single-acquisition positron emission tomography studies. *J. Cereb. Blood Flow Metab.* 21, 1480–1492.

Köhler, C., Hall, H., Ogren, S.O., Gawell, L., 1985. Specific in vitro and in vivo binding of 3H-raclopride. A potent substituted benzamide drug with high affinity for dopamine D-2 receptors in the rat brain. *Biochem. Pharmacol.* 34, 2251–2259.

Lammertsma, A.A., Hume, S.P., 1996. Simplified reference tissue model for PET receptor studies. *Neuroimage* 4, 153–158.

Lammertsma, A.A., Bench, C.J., Hume, S.P., Osman, S., Gunn, K., Brooks, D.J., Frackowiak, R.S., 1996. Comparison of methods for analysis of clinical [<sup>11</sup>C]raclopride studies. *J. Cereb. Blood Flow Metab.* 16, 42–52.

Laruelle, M., Iyer, R.N., al-Tikriti, M.S., Zea-Ponce, Y., Malison, R., Zoghbi, S.S., Baldwin, R.M., Kung, H.F., Charney, D.S., Hoffer, P.B., Innis, R.B., Bradberry, C.W., 1997. Microdialysis and SPECT measurements of amphetamine-induced dopamine release in nonhuman primates. *Synapse* 25, 1–14.

Logan, J., Fowler, J.S., Volkow, N.D., Ding, Y.S., Wang, G.J., Alexoff, D.L., 2001. A strategy for removing the bias in the graphical analysis method. *J. Cereb. Blood Flow Metab.* 21, 307–320.

Millet, P., Delforge, J., Mauguire, F., Pappata, S., Cinotti, L., Frouin, V., Samson, Y., Bendriem, B., Syrota, A., 1995. Parameter and index images of benzodiazepine receptor concentration in the brain. *J. Nucl. Med.* 36, 1462–1471.

Mintun, M.A., Raichle, M.E., Kilbourn, M.R., Wooten, G.F., Welch, M.J., 1984. A quantitative model for the in vivo assessment of drug binding sites with positron emission tomography. *Ann. Neurol.* 15, 217–227.

Morris, E.D., Babich, J.W., Alpert, N.M., Bonab, A.A., Livni, E., Weise, S., Hsu, H., Christian, B.T., Madras, B.K., Fischman, A.J., 1996a. Quantification of dopamine transporter density in monkeys by dynamic PET imaging of multiple injections of <sup>11</sup>C-CFT. *Synapse* 24, 262–272.

Morris, E.D., Alpert, N.M., Fischman, A.J., 1996b. Comparison of two compartmental models for describing receptor ligand kinetics and receptor availability in multiple injection PET studies. *J. Cereb. Blood Flow Metab.* 16, 841–853.

Muzic, R.R., Nelson, A.D., Saidel, G.M., Miraldi, F., 1996. Optimal experiment design for PET quantification of receptor concentration. *IEEE Trans. Med. Imaging* 15, 2–12.

Yoder, K.K., Wang, C., Morris, E.D., 2004. Change in binding potential as a quantitative index of neurotransmitter release is highly sensitive to relative timing and kinetics of the tracer and the endogenous ligand. *J. Nucl. Med.* 45, 903–911.

Watabe, H., Endres, C.J., Breier, A., Schmall, B., Eckelman, W.C., Carson, R.E., 2000. Measurement of dopamine release with continuous infusion of [<sup>11</sup>C]raclopride: optimization and signal-to-noise considerations. *J. Nucl. Med.* 41, 522–530.

Watabe, H., Ohta, Y., Teramoto, N., Miyake, Y., Kurokawa, M., Yamamoto, A., Ose, Y., Hayashi, T., Iida, H., 2006. A novel reference tissue approach for multiple injections of [<sup>11</sup>C]raclopride. *Neuroimage* 31 (Suppl. 2), T73.

Zhou, Y., Chen, M.K., Endres, C.J., Ye, W., Brasic, J.R., Alexander, M., Crabb, A.H., Guilarte, T.R., Wong, D.F., 2006. An extended simplified reference tissue model for the quantification of dynamic PET with amphetamine challenge. *Neuroimage* 33, 550–563.

# Influence of residual oxygen-15-labeled carbon monoxide radioactivity on cerebral blood flow and oxygen extraction fraction in a dual-tracer autoradiographic method

Katsuhiko Iwanishi · Hiroshi Watabe ·  
Takuya Hayashi · Yoshinori Miyake ·  
Kotaro Minato · Hidehiro Iida

Received: 14 December 2008 / Accepted: 8 January 2009  
© The Japanese Society of Nuclear Medicine 2009

## Abstract

**Objective** Cerebral blood flow (CBF), cerebral metabolic rate of oxygen (CMRO<sub>2</sub>), oxygen extraction fraction (OEF), and cerebral blood volume (CBV) are quantitatively measured with PET with <sup>15</sup>O gases. Kudomi et al. developed a dual tracer autoradiographic (DARG) protocol that enables the duration of a PET study to be shortened by sequentially administrating <sup>15</sup>O<sub>2</sub> and C<sup>15</sup>O<sub>2</sub> gases. In this protocol, before the sequential PET scan with <sup>15</sup>O<sub>2</sub> and C<sup>15</sup>O<sub>2</sub> gases (<sup>15</sup>O<sub>2</sub>-C<sup>15</sup>O<sub>2</sub> PET scan), a PET scan with C<sup>15</sup>O should be preceded to obtain CBV image. C<sup>15</sup>O has a high affinity for red blood cells and a very slow washout rate, and residual radioactivity from C<sup>15</sup>O might exist during a <sup>15</sup>O<sub>2</sub>-C<sup>15</sup>O<sub>2</sub> PET scan. As the current DARG method assumes no residual C<sup>15</sup>O radioactivity before scanning, we performed computer simulations to evaluate the influence of the residual C<sup>15</sup>O radioactivity on the accuracy of measured CBF and OEF values with DARG method and also proposed a subtraction technique to minimize the error due to the residual C<sup>15</sup>O radioactivity.

**Methods** In the simulation, normal and ischemic conditions were considered. The <sup>15</sup>O<sub>2</sub> and C<sup>15</sup>O<sub>2</sub> PET count curves with the residual C<sup>15</sup>O PET counts were generated by the arterial input function with the residual C<sup>15</sup>O radioactivity. The amounts of residual C<sup>15</sup>O radioactivity were varied by changing the interval between the C<sup>15</sup>O PET scan and <sup>15</sup>O<sub>2</sub>-C<sup>15</sup>O<sub>2</sub> PET scan, and the absolute inhaled radioactivity of the C<sup>15</sup>O gas. Using the simulated input functions and the PET counts, the CBF and OEF were computed by the DARG method. Furthermore, we evaluated a subtraction method that subtracts the influence of the C<sup>15</sup>O gas in the input function and PET counts.

**Results** Our simulations revealed that the CBF and OEF values were underestimated by the residual C<sup>15</sup>O radioactivity. The magnitude of this underestimation depended on the amount of C<sup>15</sup>O radioactivity and the physiological conditions. This underestimation was corrected by the subtraction method.

**Conclusions** This study showed the influence of C<sup>15</sup>O radioactivity in DARG protocol, and the magnitude of the influence was affected by several factors, such as the radioactivity of C<sup>15</sup>O, and the physiological condition.

**Keywords** PET · OEF · CBV · Carbon monoxide

K. Iwanishi (✉) · H. Watabe · T. Hayashi · H. Iida  
Department of Investigative Radiology, National Cardiovascular  
Center Research Institute, 5-7-1 Fujishirodai,  
Suita, Osaka 565-8565, Japan  
e-mail: kiwanish@ri.nccvc.go.jp

Y. Miyake  
Department of Radiology and Nuclear Medicine,  
National Cardiovascular Center, Osaka, Japan

K. Iwanishi · K. Minato  
Infomatics Science, Nara Institute of Science and Technology,  
Nara, Japan

## Introduction

Positron emission tomography with <sup>15</sup>O gas can quantitatively measure cerebral blood flow (CBF), oxygen extraction fraction (OEF), cerebral metabolic rate of oxygen (CMRO<sub>2</sub>), and cerebral blood volume (CBV). These functional values are important clinical indices that can be used to evaluate ischemic degree mainly in chronic cerebral arterial occlusive diseases. Several quantitative approaches

have been developed to obtain CBF and CMRO<sub>2</sub> images based on a single-tissue compartment model for oxygen and water kinetics [1–4]. In the steady-state method [5–9], quantitative images are estimated from data acquired while in the steady state reached during the continuous inhalation of <sup>15</sup>O<sub>2</sub> and C<sup>15</sup>O<sub>2</sub>. The study period with this method is long (approximately 2 h) due to the waiting time needed to reach equilibrium. The autoradiographic method, which uses separate administrations of three traces of CO, CO<sub>2</sub>, and O<sub>2</sub> (three-step ARG), has also been employed [3, 10–14]. The study period with the ARG method is shorter than that need with the steady-state method. However, a study with the ARG method still takes more than half an hour, because there is a waiting time for the decay of the residual radioactivity of the preceding tracer used.

Previously, Kudomi et al. developed a dual tracer autoradiographic (DARG) method to shorten the PET study period [15, 16]. This method used a single PET scan with sequential administration of dual tracers of <sup>15</sup>O<sub>2</sub> and C<sup>15</sup>O<sub>2</sub> (<sup>15</sup>O<sub>2</sub>–C<sup>15</sup>O<sub>2</sub> scan), and computed CBF and CMRO<sub>2</sub> simultaneously in an autoradiographic manner. Although the DARG approach eliminated the waiting time of radioactivity decay between <sup>15</sup>O<sub>2</sub> and C<sup>15</sup>O<sub>2</sub> administrations, a separate PET scan with C<sup>15</sup>O is required for obtaining a CBV image and correction of blood volume in CMRO<sub>2</sub> before the DARG scan. However, between these scans for C<sup>15</sup>O and the DARG we need another waiting time for the radioactivity decay of C<sup>15</sup>O, since the DARG approach itself does not take into account the residual C<sup>15</sup>O radioactivity in the arterial input function (AIF) and PET data. Furthermore, CO has a relatively long biological clearance from the blood due to high affinity to hemoglobin. While it is desired to further decrease the waiting time for the decay in the actual clinical study, it has not been defined how long it should be, and how small amount of the residual activity will affect the accuracy of CBF and CMRO<sub>2</sub>.

In this study, we performed computer simulations and evaluated the influence of this residual C<sup>15</sup>O radioactivity on the CBF and OEF values obtained by the DARG method. Moreover, we proposed a method to remove the influence of the C<sup>15</sup>O on the DARG method calculation (Subtraction method).

## Materials and methods

### Computation of functional values

CBF and OEF values were calculated from tissue TAC [ $C_i(t)$ ] and AIF during an <sup>15</sup>O<sub>2</sub>–C<sup>15</sup>O<sub>2</sub> scan, based on a single-tissue compartment model for oxygen and water, and the DARG method [15]. Using the method developed by

Kudomi et al. [16], the AIF was separated into <sup>15</sup>O<sub>2</sub> ( $A_{O_2}(t)$ ) and H<sub>2</sub><sup>15</sup>O ( $A_{H_2O}(t)$ ) (Note that although we used C<sup>15</sup>O<sub>2</sub> gas, we used H<sub>2</sub><sup>15</sup>O for the expression in this section due to the rapid exchange of H<sub>2</sub><sup>15</sup>O by carbonate dehydratase in the lung). The total radioactivity in the tissue after the <sup>15</sup>O<sub>2</sub> and C<sup>15</sup>O<sub>2</sub> administration can be expressed as,

$$C_i(t) = f \cdot A_{H_2O}(t) \otimes \exp^{-\frac{t}{p}} + E \cdot f \cdot A_{O_2}(t) \otimes \exp^{-\frac{t}{p}} + V_B \cdot R_{Hct}(1 - F_v \cdot E)A_{O_2}(t) \quad (1)$$

where  $f$  is CBF,  $E$  is the OEF,  $p$  is the blood/tissue partition coefficient of water,  $R_{Hct}$  is the small-to-large vessel hematocrit ratio, and  $V_B$  is the cerebral blood volume.  $F_v$  is the effective venous fraction. The first term of the right-hand side describes the amount of water entering the tissue. The second term represents the amount of oxygen that enters the tissue and is immediately metabolized to water. The third term is the radioactivity of the <sup>15</sup>O<sub>2</sub> in the blood vessels.

$V_B$  is separately calculated using data from a C<sup>15</sup>O scan and the following equation [13]:

$$V_B = \frac{C_{CO}}{R_{Hct} \cdot \rho_{brain} \cdot RI_{CO} \cdot \rho_{blood}} \quad (2)$$

$\rho_{brain}$  and  $\rho_{blood}$  represent the densities of blood (=1.06 g/mL) and brain tissue (=1.04 g/mL).  $RI_{CO}$  (Bq/mL) is the mean of the radioactivity concentration for C<sup>15</sup>O in the arterial blood.

To calculate functional values using a look-up table procedure, Eq. 1 was integrated for the periods after the H<sub>2</sub><sup>15</sup>O (represents  $\int_w$ ) and <sup>15</sup>O<sub>2</sub> administration (represents  $\int_o$ ) as

$$\int_w C_i(t) dt = f \int_w A_{H_2O}(t) \otimes \exp^{-\frac{t}{p}} dt + E \cdot f \int_w A_{O_2}(t) \otimes \exp^{-\frac{t}{p}} dt + V_B \cdot R_{Hct}(1 - F_v \cdot E) \int_w A_{O_2}(t) dt \quad (3)$$

$$\int_o C_i(t) dt = f \int_o A_{H_2O}(t) \otimes \exp^{-\frac{t}{p}} dt + E \cdot f \int_o A_{O_2}(t) \otimes \exp^{-\frac{t}{p}} dt + V_B \cdot R_{Hct}(1 - F_v \cdot E) \int_o A_{O_2}(t) dt$$

From the above equation,  $E$  can be expressed as follows:

$$E = \frac{\int_o C_i(t) dt - f \int_o A_{H_2O} \otimes \exp^{-\frac{t}{p}} dt - V_B \cdot R_{Hct} \int_o A_{O_2} dt}{f \int_o A_{O_2} \otimes \exp^{-\frac{t}{p}} dt - V_B \cdot R_{Hct} \cdot F_v \int_o A_{O_2} dt} \quad (4)$$

Substituting Eq. 4 into Eq. 3, we obtain

$$\int_w Ci(t)dt = f \int_w A_{H_2O}(t) \otimes \exp^{-\frac{t}{T}} dt + V_B \cdot R_{Hct} \int_w A_{O_2}(t)dt + \left( f \int_w A_{O_2}(t) \otimes \exp^{-\frac{t}{T}} dt - V_B \cdot R_{Hct} \cdot Fv \int_w A_{O_2}(t)dt \right) \times \frac{\int_o Ci(t) - f \int_o A_{H_2O} \otimes \exp^{-\frac{t}{T}} dt - V_B \cdot R_{Hct} \int_o A_{O_2} dt}{f \int_o A_{O_2} \otimes \exp^{-\frac{t}{T}} dt - V_B \cdot R_{Hct} \cdot Fv \int_o A_{O_2} dt} \quad (5)$$

Using Eq. 5,  $f$  can be estimated using a look-up table procedure based on the integration value of the tissue TAC and separated input function. Next,  $E$  can be calculated using Eq. 4.

Study protocol with DARG method

Figure 1 shows a schematic diagram of the clinical study protocol with the DARG method for our institute. The PET scanner we used was an ECAT EXACT47 (CTI Inc., Knoxville, USA). First, a 10 min transmission scan was performed to correct for gamma ray attenuation. Then gaseous  $C^{15}O$  of 2500 MBq was inhaled for 30 s, and 90 s post-inhalation, a 4 min emission scan ( $C^{15}O$  scan) was performed to obtain a CBV image. Finally, a single dynamic PET scan was conducted during the sequential administration of gaseous  $^{15}O_2$  (4000 MBq) and  $C^{15}O_2$  (5000 MBq) in a short time interval. Their inhalation times were 1 min.

A catheter was inserted into the brachial artery of the patient. The arterial blood was sampled at the beginning of

the  $C^{15}O$  scan for 30 s and the radioactivity concentration in the arterial blood was measured by a Well counter system (Shimadzu Corporation, Kyoto, JAPAN). In order to obtain the AIF, the radioactivity in the arterial blood during a  $^{15}O_2-C^{15}O_2$  scan was continuously monitored by a GSO detector [17] with a flow rate of 3.5 mL/min. The inner diameter of the tube was approximately 2 mm, and the distance from the catheter to the detector was 20–25 cm.

Residual  $C^{15}O$  radioactivity

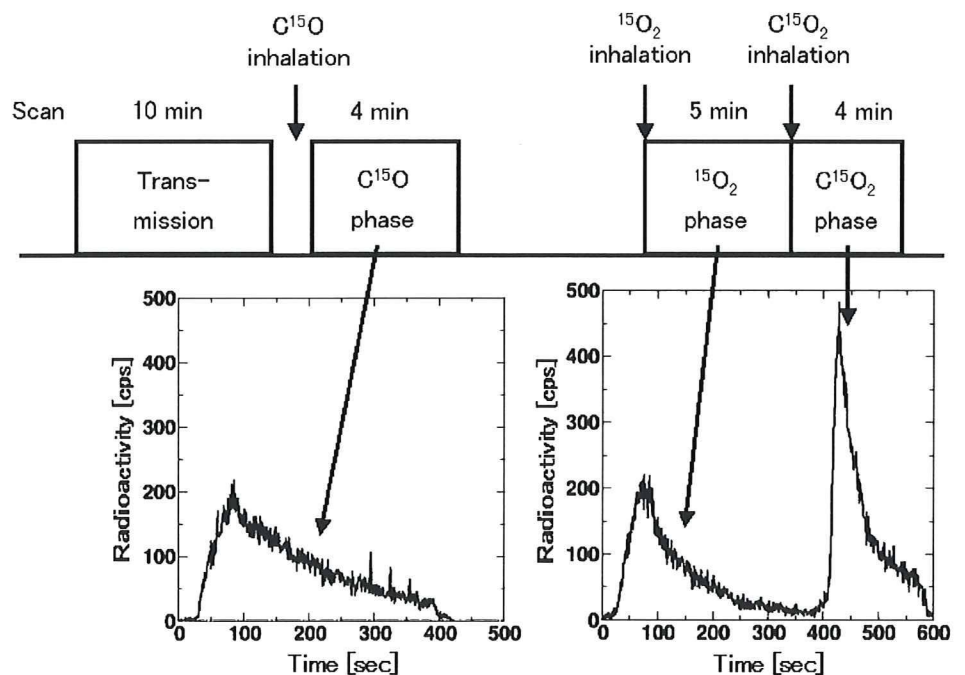
As described in the “Introduction”, the AIF and PET counts obtained during a DARG study may be contaminated by residual  $C^{15}O$  radioactivity. By assuming that the  $C^{15}O$  was physically decayed but not biologically cleared, the radioactivity of the  $C^{15}O$  in the AIF and PET counts during the  $O_2-CO_2$  scan could be quantified. The residual radioactivity of the  $C^{15}O$  [ $R_{CO}(0)$  (Bq/mL)] in the AIF at the start time of the  $O_2-CO_2$  can be written as follows:

$$R_{CO} = A_{CO} \cdot \exp(-\lambda T), \quad (6)$$

where  $A_{CO}$  (Bq/mL) is the measured arterial radioactivity for  $C^{15}O$  by the Well counter and  $\lambda$  is the physical decay constant for  $^{15}O$  ( $0.005670 s^{-1}$ ).

PET counts from the residual  $C^{15}O$  ( $C_{CO}$ ) were calculated from  $R_{CO}$  and the measured CBV ( $V_B$ ) by  $C^{15}O$  scan from Eq. 2 as follows

Fig. 1 Schematic diagram of PET study with DARG method protocol. After a 10 min transmission scan,  $C^{15}O$  gas is inhaled for 30 s before the start of a 4 min scan. There is approximately 10 min in the administration interval for  $C^{15}O$  and  $^{15}O_2$ . Next, a 9 min single scan with sequential administration of  $^{15}O_2$  and  $C^{15}O_2$  is performed. The administration interval between  $^{15}O_2$  and  $C^{15}O_2$  is 300 s. The graphs below are arterial input functions without corrections for decay, delay, and scaling for  $C^{15}O$  (left),  $^{15}O_2$  and  $C^{15}O_2$  (right)



$$C_{CO} = R_{CO} \cdot \rho_{\text{blood}} \cdot \rho_{\text{brain}} \cdot R_{\text{Hct}} \cdot V_B. \quad (7)$$

We proposed a subtraction method that eliminates the influence of the  $C^{15}O$  radioactivity in both the AIF and PET counts during the  $O_2$ - $CO_2$  scan. The true AIF ( $A_{\text{True}}$ ) of the  $^{15}O_2$ - $C^{15}O_2$  at time  $t$  was obtained by subtracting  $R_{CO}$  from the measured whole radioactivity [ $A_{\text{Whole}}(t)$ ], i.e.,  $A_{\text{True}}(t) = A_{\text{Whole}}(t) - R_{CO}$ .  $(8)$

Note that  $A_{\text{True}}(t)$  and  $A_{\text{Whole}}(t)$  were corrected for the physical decay of  $^{15}O$  against the scan start time 0. PET counts without the residual CO radioactivity could be obtained by subtracting  $C_{co}$  in Eq. (7) from the observed PET counts as follows:

$$C_{\text{True}}(t) = C_i(t) - C_{co}. \quad (9)$$

Using  $A_{\text{True}}(t)$  and  $C_{\text{True}}(t)$ , CBF and OEF were calculated in the DARG manner.

### Simulation studies

As shown in Eq. 1, DARG calculation does not take into account the residual radioactivity of the CO. However, in an actual situation, both the PET count [ $C_i(t)$ ] and the input function ( $A_{O_2}$  and  $A_{H_2O}$ ) might contain radioactivity from the  $C^{15}O$ . So, the CBF and OEF values calculated by the DARG method are influenced by the  $C^{15}O$  radioactivity, causing error and noise in the terms of Eq. 1. Computer simulations were performed to evaluate this influence. Both normal and ischemic models were considered in these simulations. Moreover, the effect of the subtraction method was examined.

The simulations were performed using a PC [CPU: Intel (R) Pentium (R) 4 2.80 GHz, OS: Linux Fedora Core 7] with a PyBLD environment [18].

### Simulated input function with CO radioactivity

We used a typical arterial input function from one patient's data for the simulations. From the measured input function, the input functions with  $C^{15}O$  radioactivity (combined input function, CIF) were generated using Eq. 6. The amount of residual  $C^{15}O$  radioactivity was varied by changing two conditions, the time lag between the  $C^{15}O$  scan and the  $^{15}O_2$ - $C^{15}O_2$  scan ( $T$  in Eq. 6), and the  $C^{15}O$  radioactivity against the  $^{15}O_2$  radioactivity ( $A_{co}$  in Eq. 6). The time lags selected were 60, 100, 200, 400, and 800 s, and the inhaled  $C^{15}O$  radioactivity was either 25% (case '25%') or 100% (case '100%') of the  $^{15}O_2$  inhaled radioactivity. 100 sets of noisy arterial TACs for  $C^{15}O$  were realized by assuming that the standard deviation of the  $C^{15}O$  radioactivity was equal to the square root of the  $C^{15}O$  radioactivity. Figure 2 (left) shows the CIF after  $^{15}O_2$  gas inhalation in a case where the time lag was 60 s. These TACs did not correct the physiological decay of  $^{15}O_2$ . For the subtraction method,  $A_{\text{True}}(t)$  in Eq. 8 was computed for each dataset.

### Simulated tissue TAC with CO radioactivity

Using the typical input function and Eq. 1, the tissue TAC during a  $^{15}O_2$ - $C^{15}O_2$  scan was simulated. We considered two physiological conditions, namely the normal condition

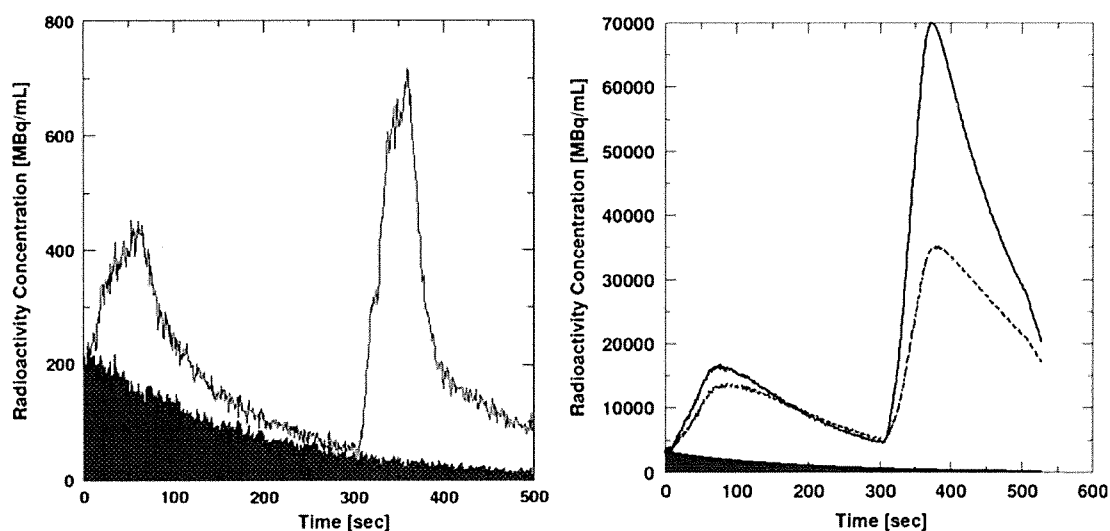


**Fig. 2** Input function (left) and PET count curves (right) during the  $^{15}O_2$ - $C^{15}O_2$  scan. These curves have the added residual  $C^{15}O$  radioactivity (hatched region). The interval time for the  $C^{15}O$  and  $^{15}O_2$  is 60 s, and the inhaled  $C^{15}O$  radioactivity is 100% of the peak

value for  $^{15}O_2$ .  $C^{15}O$  time-activity curve. The solid line in the right graph indicates the PET counts in the normal model, and the dashed line is the PET counts in the ischemic model

(CBF = 0.5 mL/g tissue/min, OEF = 0.4, CBV = 0.04, mL/g,  $p = 0.8$  mL/g,  $F_v = 0.835$ , and  $R_{Hct} = 0.85$ ) and an ischemic condition (CBF = 0.2 mL/g tissue/min, OEF = 0.7, CBV = 0.04 mL/g,  $p = 0.8$  mL/g,  $F_v = 0.835$ , and  $R_{Hct} = 0.85$ ). The tissue radioactivity from the residual  $C^{15}O$  radioactivity was added to the simulated tissue TACs using Eq. 7. 100 sets of noisy tissue TACs were generated using an NEC model [19]. Figure 2 (right) shows a simulated tissue TAC under the condition of a time lag of 60 s and the case '100%'. For the subtraction method,  $C_{True}(t)$  in Eq. 9 was computed for each dataset.

#### Calculation and evaluation of CBF and OEF values

The  $H_2^{15}O$  contents ( $A_{H_2O}$ ) and  $^{15}O_2$  contents ( $A_{O_2}$ ) were separated from the input functions using the separation method proposed by Kudomi et al. [16]. This separation is

demonstrated in Fig. 3. The CBF and OEF values were computed from the  $A_{H_2O}$ ,  $A_{O_2}$ , and the tissue TACs by means of Eqs. 4 and 5. The errors, in the form of bias and coefficient of variance (COV), in the estimated CBF and OEF values were calculated by comparing them with the true CBF and OEF values.

#### Results

Tables 1 and 2 show the results of the estimated values and COV for CBF and OEF in this simulation study using the conventional DARG method in the cases of the normal model and ischemic model, respectively. As shown in these tables, the estimated CBF and OEF values were underestimated in all cases due to the residual  $C^{15}O$  radioactivity. For instance, in the case of the normal model and a time lag of 60 s, the underestimation of the estimated OEF value

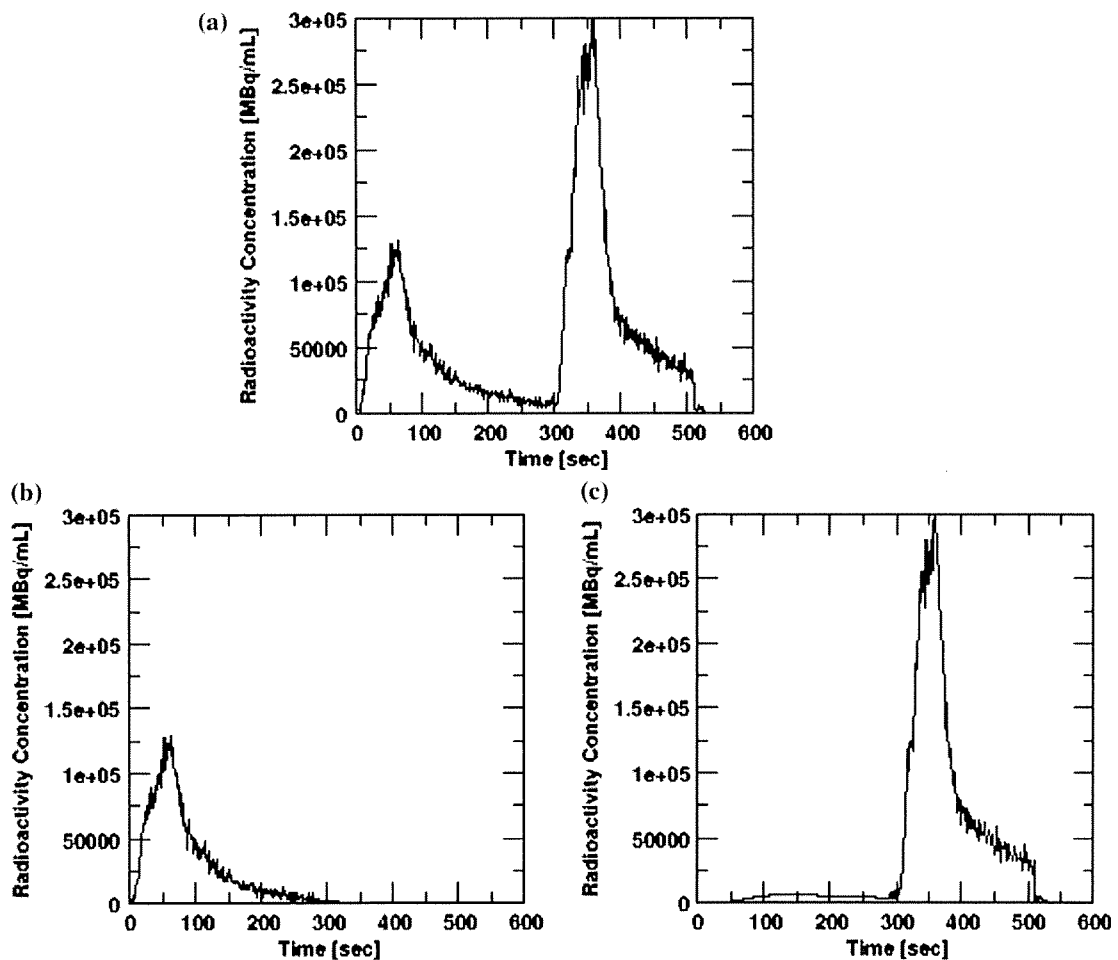


Fig. 3 Separation of the input function for the  $^{15}O_2$ - $C^{15}O_2$  scan. Total input function (a),  $^{15}O_2$  input function (b), and  $C^{15}O_2$  input function (c) separated from the total input function. The radioactivity observed earlier than 300 s in the graph (c) is the recirculation water

**Table 1** Summary of simulation for CBF and OEF in the case '25%' and the case '100%' of the normal model using the conventional DARG method

$C^{15}O-^{15}O_2$ time lag (s)	CBF			OEF		
	Average (mL/g/min)	Error (%)	COV (%)	Average	Error (%)	COV (%)
Case '25%'						
60	0.49	-2.06	1.07	0.30	-25.0	1.06
100	0.49	-1.82	0.66	0.31	-21.0	0.52
200	0.50	-0.12	0.23	0.35	-13.5	0.33
400	0.50	-0.04	0.17	0.38	-4.55	0.19
800	0.50	-0.02	0.06	0.40	-0.48	0.07
Case '100%'						
60	0.46	-7.55	1.68	0.16	-60.9	1.64
100	0.47	-6.05	1.37	0.18	-54.4	1.25
200	0.48	-3.91	0.92	0.25	-38.7	0.823
400	0.49	-1.51	0.42	0.34	-16.0	0.45
800	0.50	-0.19	0.08	0.39	-1.90	0.12

**Table 2** Summary of simulation for CBF and OEF in the case '25%' and the case '100%' of ischemic model using the conventional DARG method

$C^{15}O-^{15}O_2$ time lag (s)	CBF			OEF		
	Average (mL/g/min)	Error (%)	COV (%)	Average	Error (%)	COV (%)
Case '25%'						
60	0.20	-2.72	0.30	0.55	-21.3	0.48
100	0.20	-2.18	0.26	0.58	-17.8	0.37
200	0.20	-1.30	0.17	0.62	-10.9	0.30
400	0.20	-0.45	0.07	0.67	-3.83	0.16
800	0.20	-0.04	0.02	0.70	-0.39	0.06
Case '100%'						
60	0.18	-8.27	0.88	0.33	-52.6	1.08
100	0.19	-6.84	0.71	0.37	-46.9	0.85
200	0.19	-4.43	0.43	0.47	-33.1	0.62
400	0.20	-1.70	0.18	0.61	-13.6	0.36
800	0.20	-0.20	0.04	0.69	-1.60	0.11

was -25% for the case '25%' and -61% for the case '100%'. Larger underestimation values were observed for shorter time lags. The OEF estimation was more sensitive to the residual CO radioactivity than the CBF estimation. Less underestimation was observed in the CBF value in the normal model than in the ischemic model. On the other hand, a larger underestimation was observed in the OEF value in the normal model compared to the ischemic model. The COV was always larger in the normal model than in the ischemic model.

Tables 3 and 4 show the results of the estimated values and the COV for CBF and OEF using the subtraction method. As shown in the tables, no underestimation was observed in all cases. Moreover, the COV values were less than one by the conventional method.

## Discussion

CBV images are widely used for the diagnosis of cerebrovascular disease [20]. These images are also utilized to correct the vascular space in the DARG method for CBF and OEF values [15]. Therefore, a  $C^{15}O$  scan is mandatory for the DARG protocol. Due to a desire to shorten the total study period, it is often observed that the  $^{15}O_2-C^{15}O_2$  scan is initiated without waiting long enough for the physical decay of the  $C^{15}O$  radioactivity. In this paper, the influences of this residual  $C^{15}O$  radioactivity on the CBF and OEF values for the DARG protocol were evaluated by means of computer simulations. According to the results, the CBF and OEF values were underestimated because of the residual  $C^{15}O$  radioactivity. The magnitude of the